Lipid hydrogen isotope compositions primarily reflect growth water in the model archaeon *Sulfolobus acidocaldarius*

Carolynn M. Harris[a#], Sebastian Kopf[b], Jeemin H. Rhim[a,c], Alec Cobban[a], Felix J. Elling[d,e], Xiahong Feng[a], Jamie McFarlin[b,f], Yuki Weber[,d^], Yujiao Zhang[a%], Alice Zhou[a&], Harpreet Batther[b], Ann Pearson[d], William D. Leavitt [a,g]

[a] Department of Earth Sciences, Dartmouth College

[b] Department of Geological Sciences, University of Colorado at Boulder

[c] Department of Ecology, Evolution, and Marine Biology, U.C. Santa Barbara

[d] Department of Earth & Planetary Sciences, Harvard University

[e] Leibniz-Laboratory for Radiometric Dating and Isotope Research, Kiel University

[f] Department of Geology and Geophysics, University of Wyoming

[g] Department of Chemistry, Dartmouth College

Running head: Lipid hydrogen isotopes of S. acidocaldarius

Address correspondence to Carolynn M. Harris, carolynn.m.harris.gr@dartmouth.edu

[&] Current address: Connecticut Agricultural Experiment Station, New Haven, CT

[^] Current address: Chroma Medicine, Boston, MA

[%] Current address: National Center for Science & Technology Evaluation, P.R. China

Abstract

The stable hydrogen isotope composition (δ^2H) of lipid biomarkers can track environmental processes and remain stable over geologically relevant time scales, enabling studies of past climate, hydrology, and ecology. Most research has focused on lipids from the domain Eukarya (e.g., plant waxes, long-chain alkanes), and the potential of prokaryotic lipid biomarkers from the domain Archaea to offer unique insights into environments not captured by eukaryotic lipids remains unclear. Here, we investigate the H-isotope composition of biphytanes in *Sulfolobus acidocaldarius*, a model thermoacidophile and obligate heterotroph. We conducted a series of experiments that varied temperature, pH, shaking rate, electron acceptor availability, or electron donor flux. From these experiments, we quantified the lipid/water H-isotope fractionation ($^2\varepsilon_{L/W}$) values for core biphytane chains derived from tetraether lipids. The $^2\varepsilon_{L/W}$ values are consistently negative (-230 to -180 ‰) and are relatively invariant across all experiments despite the 20-fold change in doubling times and 2-fold change in lipid cyclization. The magnitude and relative invariance of $^2\varepsilon_{L/W}$ values are consistent with studies on other heterotrophic archaea and suggests archaeal lipids may be faithful recorders of the δ^2H composition of growth water. Our study highlights the potential of archaeal lipid $^2\varepsilon_{L/W}$ as a hydrological proxy, offering new insights into environments where traditional proxies, such as plant-derived lipids, are not available, including extreme environments and extraterrestrial settings.

Importance

Reconstructing past climates is crucial for understanding Earth's environmental history and its responses to changing conditions. This study examines *Sulfolobus acidocaldarius*, a thermoacidophilic archaeon that thrives in extreme environments like hot springs. These microorganisms incorporate hydrogen from their growth water into membrane lipids, creating hydrogen isotope signatures that can reflect hydroclimate conditions. Our findings show that these hydrogen isotope ratios remain consistent even under varying temperature, pH, oxygen levels, and electron donor fluxes, indicating a stable fractionation between lipids and water. This invariance suggests that *S. acidocaldarius* lipids could serve as a robust proxy for reconstructing ancient water H-isotope values, especially in extreme environments where traditional proxies, such as plant waxes, are absent. This research has broader implications for planetary-scale reconstructions, including potential applications in studying past climates on other planets, such as Mars, where similar microorganisms may have existed in hydrothermal or acidic conditions.

1. Introduction

The relative abundances of hydrogen isotopes ($^2H/^1H$) in water are set by physical, hydrological, and climatic factors(Gat 1996; Hayes 2001). Certain biomolecules incorporate these isotopes with a consistent offset (fractionation) relative to water, preserving a record of the isotopic composition (δ^2H values) of the water present during growth (Sessions et al. 1999). Some lipids can retain their original H-isotope composition for up to 10^8 years and lipid hydrogen isotope compositions have been used to study hydrologic and environmental change over millennia to millions of years, dating as far back as the Paleoproterozoic (Sessions et al. 2004; Dawson et al. 2004; Sachse et al. 2012; Sessions 2016; Liu and An 2019; McFarlin et al. 2019; Ladd et al. 2021; Love and Zumberge 2021). Most studies of biomarker H-isotope composition focus on lipids from photoautotrophic organisms (e.g., plant wax *n*-alkanes) or chemoautotrophic and heterotrophic bacteria (e.g., fatty acids) (Sessions et al. 1999; Zhang et al. 2009a; Osburn et al. 2011; Dawson et al. 2015; Sachs and Kawka 2015; Osburn et al. 2016; Maloney et al. 2016; Sachs et al. 2017) and the H-isotope compositions recorded in lipids from the Archaea are comparatively poorly understood. A small, but growing, body of literature, however, has begun to address this gap (Kaneko et al. 2011; Dirghangi and Pagani 2013; Lengger et al. 2020; Wu et al. 2020; Leavitt et al. 2023; Rhim et al. 2024). Understanding the extent to which lipid δ^2H in archaea records the δ^2H of growth water requires a deeper examination of how environmental conditions impact this signal. A comprehensive investigation of the physicochemical factors affecting H-isotope fractionation between archaeal lipids and water ($^2\varepsilon_{L/W}$) is essential for employing archaeal lipid δ^2H as a proxy for environmental water δ^2H over space and time.

The $^2\varepsilon_{L/W}$ value for a biomolecule integrates both the composition of source water and the net biosynthetic fractionations resulting from the specific pathways used during lipid biosynthesis. Reported $^2\varepsilon_{L/W}$ values vary widely among domains of life. In Eukaryotes, experimental calibrations of $^2\varepsilon_{L/W}$ in waxes (e.g., n-alkanes) from plants and algae show that net biosynthetic fractionation is generally consistent across taxa (Sachs and Kawka 2015), though genetic factors introduce some variance (Bender et al. 2016). Environmental factors such as temperature, salinity, irradiance, and CO_2 concentration, also influence $^2\varepsilon_{L/W}$ values, possibly via their impact on growth and biosynthesis rates (Sachs 2014; Sachs and Kawka 2015; Van Der Meer et al. 2015; Sachs et al. 2016; Maloney et al. 2016; Wolfshorndl et al. 2019; Torres-Romero et al. 2024) . These effects are well-characterized in plants, and to a lesser extent in algae, and can be accounted for when plant wax δ^2H is used as a proxy in paleohydroclimate studies (Sachse et al. 2012; Sessions 2016; McFarlin et al. 2019).

In contrast to the relatively consistent $^2\varepsilon_{L/W}$ values observed in phototrophic eukaryotes, experimental investigations of bacterial fatty acids reveal that $^2\varepsilon_{L/W}$ varies widely in direction and magnitude (-400 ‰ to +300 ‰) (Sessions et al. 2002; Valentine 2009; Zhang et al. 2009a; Dawson et al. 2015; Leavitt 2016; Osburn et al. 2016; Leavitt et al. 2017; Wijker et al. 2019). Bacteria using different energy capture strategies (e.g., chemoautotrophy, photoautotrophy, or heterotrophy) exhibit distinct ranges of $^2\varepsilon_{L/W}$ values, which has been attributed to differences in metabolic

pathways and the substrate used for growth (e.g., simple sugars vs. tricarboxylic acid (TCA) cycle intermediates). A recent synthesis suggests that variations in $^{2}\varepsilon_{L/W}$ among aerobic heterotrophic bacteria can be explained by hydrogen fluxes through intracellular hydride carriers, such as $NADP^{+}$ and NADPH (Wijker et al. 2019) Given this metabolism-dependent heterogeneity in $^{2}\varepsilon_{L/W}$, bacterial lipid $\delta^{2}H$ in sediment records have more utility as proxies for microbial metabolisms than for past hydroclimate reconstructions (Zhang et al. 2009a; Osburn et al. 2016; Wijker et al. 2019).

In the domain Archaea to-date, $^{2}\varepsilon_{L/W}$ values have been reported for diether lipids (archaeol) in a mesophilic halophile (Dirghangi and Pagani 2013) and a methanogen (Wu et al. 2020), tetraether-derived biphytanes in three thermoacidophiles and one thermomesophile (Kaneko et al. 2011; Rhim et al. 2024) and one marine obligate autotroph (Leavitt et al. 2023), and whole tetraethers or tetraether-derived biphytanes in few environmental sediment samples (Kaneko et al. 2011; Lengger et al. 2020). The observed $^{2}\varepsilon_{L/W}$ values for these archaeal lipids are uniformly negative (i.e. -300 to -150 ‰) and similar in magnitude to those reported for isoprenoid lipids produced by eukaryotic phototrophs (e.g. C_{15} and C_{30} isoprenoids; Sessions et al. 1999; Sachs et al. 2016).

Our understanding of the factors controlling the H-isotope compositions of archaeal lipids are less developed than for the Eukarya and Bacteria. Recent experiments demonstrate that $^{2}\varepsilon_{L/W}$ is nearly constant over a range of growth rates in a marine autotroph (*Nitrosopumilus maritimus*; Leavitt et al., 2023) and that the impacts of carbon metabolism and growth phase on $^{2}\varepsilon_{L/W}$ are minor (*Archaeoglobus fulgidus*; Rhim et al., 2024). This relative invariance in $^{2}\varepsilon_{L/W}$ is perhaps surprising considering the taxonomic and metabolic diversity of the investigated Archaea. The impact of environmental factors on $^{2}\varepsilon_{L/W}$, however, has only been investigated within a single archaeal strain (*Haloarcula marismortui*; Dirghangi and Pagani 2013). Further investigation of the effects of multiple environmental factors on $^{2}\varepsilon_{L/W}$ in Archaea is crucial, particularly since many archaea are adapted to extreme environments that can experience both rapid and large changes to physicochemical conditions (Van de Vossenberg et al. 1998).

Isoprenoid glycerol dibiphytanyl glycerol tetraethers (iGDGTs) are archaeal lipids with particular relevance to paleoenvironmental reconstructions (Schouten et al. 2013). These tetraethers are structurally diagnostic, diagenetically robust, and routinely analyzed for paleoclimate reconstruction based on the relative abundances of specific structural moieties (Schouten et al. 2002, 2013; Pearson and Ingalls 2013). Archaea can synthesize a unique series of iGDGTs that contain from zero to eight cyclopentane rings (e.g., iGDGT-0 through iGDGT-8), though the most highly ringed moieties (iGDGT-7 and -8) have only been recovered from hydrothermal spring environments (De Rosa and Gambacorta 1988). Members of the Thaumarchaeota phyla can also produce crenarchaeol, an iGDGT containing four cyclopentane rings and one cyclohexyl ring (De Rosa and Gambacorta 1988). The distribution of these moieties in natural systems is related to growth temperature and other environmental factors (Elling et al. 2014, 2017; Hurley et al. 2016; Cobban et al. 2020; Zhou et al. 2020) and forms the basis of the TEX_{86} paleo sea surface temperature

128 proxy (Schouten et al. 2002). At low pH and high temperatures, Archaea synthesize more highly-
129 ringed moieties as an adaptation to maintain membrane rigidity and reduce permeability. In
130 hydrothermal systems, the ring distributions of thermoacidophilic archaea record the interactions
131 between temperature, pH, energy availability, and other factors that influence growth rate (Zhou et
132 al. 2020; Quehenberger et al. 2020; Yang et al. 2023).

133 To better understand the signals recorded by archaeal lipid δ^2H in natural systems, it is necessary to
134 determine the extent to which environmental conditions influence $^2\varepsilon_{L/W}$. In this study, we determined
135 the H-isotope fractionation between iGDGT-derived biphytanes and growth water ($^2\varepsilon_{L/W}$) for the
136 thermoacidophilic and heterotrophic archaeon, *Sulfolobus acidocaldarius* (DSM 639), which is
137 capable of simultaneously coping with multiple extreme conditions (e.g., pH < 4 and temperatures
138 > 60°C). We cultured *S. acidocaldarius* under a range of environmentally relevant physicochemical
139 conditions: temperature, pH, shaking rate, electron acceptor (O_2) availability, or electron donor
140 (sucrose) flux. Changes in these environmental conditions are known to impact the growth rate and
141 degree of iGDGT cyclization (Boyd et al., 2011; Jensen et al., 2015; Zhou et al., 2019; Quehenberger
142 et al., 2020; Cobban et al., 2020), but their impact on lipid/water fractionation is unexplored. For all
143 experiments, we report $^2\varepsilon_{L/W}$ values for biphytane (BP) hydrocarbons derived via ether cleavage from
144 acid extractable iGDGTs.

145 **2. Methods**

146 **2.1 Culture strains and growth**

147 Axenic cultures of *S. acidocaldarius* (DSM 639) were grown aerobically under different
148 environmental conditions (**Table 1**). Culture media was prepared following the Brock recipe in
149 Wagner et al. (2012) with the following modifications (see *Substrate* column in Table 1). For all
150 experiments, media contained 5.9 mmol L^{-1} (0.2% w/v) sucrose as the organic substrate. The
151 electron donor flux experiments were also supplemented with 4.0 mmol L^{-1} (0.1% w/v) NZ-amine in
152 addition to sucrose.

153 Growth was monitored photometrically at regular intervals throughout each experiment by
154 measuring the optical density (i.e., absorbance at 1 cm pathlength) of a culture aliquot at 600 nm
155 (OD_{600}) on a spectrophotometer. All experiments were inoculated to an initial OD_{600} between 0.004
156 and 0.008, using cells derived from an active pre-culture (grown on the same medium) in mid-
157 exponential phase. Specific growth rates (division day^{-1}; μ) were calculated using OD_{600}
158 measurements during the early to mid exponential phase after Cobban et al., (2020). Doubling time
159 (T_D) was calculated as:

160 **Eq. (1)** $$T_D\ (hours) = ln(2)/\mu$$

161 **2.2 Experimental conditions experiments**

162 We examined how temperature, pH, shaking rate, O_2 availability, and electron donor (sucrose) flux
163 influence H-isotope fractionation in *S. acidocaldarius* through a series of batch, fed-batch, and
164 chemostat experiments.

165 **Batch experiments:** Three sub-experiments were performed in which one environmental condition
166 (temperature, pH, or shaking rate) was systematically varied while holding the other two conditions
167 constant (previously described in Cobban et al., 2020). The reference conditions were 70 °C, pH 3,
168 and 200 RPM shaking rate. Shaking rate is considered a proxy for aeration rate, where faster speeds
169 increase oxygen availability in the media.

170 Batch experiments were performed in temperature-controlled, shaking incubators (Innova-42,
171 Eppendorf) in 250 mL Erlenmeyer flasks containing 125 mL media covered with loose plastic caps to
172 reduce evaporation. Evaporation was further reduced by maintaining a 2L tray of water in the
173 incubator to humidify the atmosphere. All experiments were performed in quintuplicate. Biomass
174 samples were collected in mid-exponential phase by centrifuging (3214 x *g*; Eppendorf 5810 R, S-4-
175 104 rotor) 50 mL of culture for 15 minutes at 4 °C, the resulting cell pellets were stored at -80 °C until
176 lipid extraction.

177 **Fed-batch bioreactor experiments:** To more precisely determine the impact of oxygen availability,
178 we performed gas-fed batch experiments in bioreactors (previously described in Cobban et al.,
179 2020). Briefly, *S. acidocaldarius* was grown in 300 mL of medium in 1 L glass vessels. To modulate
180 availability (as flux) of the terminal electron acceptor O_2 was introduced to bioreactors at four
181 different partial pressures: 0.2, 0.5, 2.0 or 20 % (balance N_2). The O_2 dry mixing ratios 0.2, 0.5, and
182 2% were generated by mixing pure N_2 mixed with 2% O_2 at 9:1, 3:1, and 0:1 ratios, respectively, which
183 was controlled via my-Control PID controllers (Applikon, Delft, Netherlands). The 20% experiment
184 used a separate gas feedstock of Ultra ZeroGrade Air (AirGas). Culture conditions were maintained
185 at 70 °C, pH 3, stirred at 200 RPM (Rushton-type impeller), and at a total gas flux of 200 mL min^{-1}.
186 Each experiment was performed in triplicate via three bioreactors operated in parallel. Biomass
187 samples were collected by removing culture directly from the vessel, centrifuged at 4 °C, to pellet
188 biomass, and then stored at -80 °C until lipid extraction.

189 **Chemostat experiments:** To determine the impact of electron donor flux, we performed chemostat
190 experiments in which the dilution rate of the growth vessel was set to yield cell doubling times (T_D) of
191 7.0, 21.3, and 40.0 hours (previously described in Zhou et al. 2020). Briefly, *S. acidocaldarius* was
192 grown in 300 mL of medium maintained at 70 ºC, pH 2.25, stirred at 200 RPM (Rushton-type
193 impeller), and aerated with a constant flux of 200 mL min^{-1} Zero Air (ultra-high purity, UHP, AirGas/
194 AirLiquide, Inc.). When steady state was achieved (assessed via regular OD_{600} measurements),

biomass samples were harvested by continually collecting the outflow of each bioreactor into a chilled vessel (0 to 4 °C) for between 1 and 4 days, followed by centrifugation at 4 °C and storage at -80 °C prior to lipid processing. Multiple extracts representing 2 to 3 sampling events at identical growth rates were combined before lipid extraction.

2.3 Lipid extraction and derivatization

Core lipid fractions (iGDGTs) were extracted from lyophilized cell pellets via acidic hydrolysis-methanolysis (Elling et al. 2017; Zhou et al. 2020). iGDGTs were chemically derivatized to biphytanes to permit the determination of the δ^2H value of component biphytanes as described in Kaneko et al., (2011) and Leavitt et al., (2023). In brief, ether bonds were cleaved via digestion in 57% hydroiodic acid (HI) at 125 °C for 4 hours. The resulting alkyl iodides were hydrogenated (e.g., reduced to biphytanes, BPs) in H_2/PtO_2. An isotope dilution occurs when H is added during hydrogenation, which is corrected for during data processing and reduction (see Section 2.5).

2.4 Lipid identities & distributions

Isoprenoid BP chains were analyzed via GC-MS (Thermo ISQ LT with TRACE 1310) for compound identification and via GC-flame ionization detector (GC-FID; Thermo TRACE 1310) for compound quantification at the University of Colorado at Boulder Earth Systems Stable Isotope Lab (CUBES-SIL, Boulder, CO) (**FIG 1**). Biphytane yields and recovery were calculated using GC peak areas and co-injected n-alkane mixture as a quantification standard.

To describe the average amount of cyclopentyl rings in each BP distribution, we calculated a BP-Ring Index based on the relative abundance of each BP moiety (**Eq. 2**). This metric is similar to the iGDGT-based Ring Index (**Eq. 3**), which describes the average amount of cyclopentyl rings in a distribution based on the relative abundance of each iGDGT moiety (Zhang et al. 2016; Zhou et al. 2020).

Eq. (2)

$$RI_{BP} = \frac{BP{-}1 + (2 \cdot BP{-}2) + (3 \cdot BP{-}3)}{\sum_{o}^{3} BP}$$

Eq. (3)

$$RI_{GDGT} = \frac{iGDGT{-}1 + (2 \cdot iGDGT{-}2) + (3 \cdot iGDGT{-}3) + \ldots + (8 \cdot iGDGT{-}8)}{\sum_{o}^{8} iGDGT}$$

2.5 δ^2H analysis of media waters, substrates, and biphytane lipids

2.5.1 Media waters

The hydrogen isotope composition (δ^2H) of filter-sterilized growth medium water was measured at the end of culture experiments on 2 mL aliquots at the Stable Isotope Laboratory at Dartmouth

College via a dual inlet isotope ratio mass spectrometer (IRMS; Thermo Delta Plus 304 XL) coupled to an H-Device (pyrolyzed to H_2 gas) for water reduction by chromium powder at 850°C (previously described in Kopec et al. (2018). ^{2}H-labeled waters were diluted with standards of known isotopic composition prior to analysis. The δ^2H_{Water} values were corrected using laboratory standards relative to VSMOW. Analytical precision was <0.5 ‰.

2.5.2 Substrates

The δ^2H composition of non-exchangeable C-bound H from substrates used in growth media was analyzed in triplicate as trifluoroacetate derivatives via a Thermo Delta Plus XP coupled to a TC-EA (Abrahim et al. 2020). The δ^2H composition of sucrose was -93.0 ± 1.2 ‰.

2.5.3 Biphytanes

The δ^2H composition of individual BPs was determined by gas chromatography pyrolysis isotope ratio mass spectrometry (GC-P-IRMS) on a GC IsoLink II IRMS System (Thermo Scientific) at the University of Colorado at Boulder Earth Systems Stable Isotope Lab (CUBES-SIL, Boulder, CO). The system comprised a Trace 1310 GC fitted with a programmable temperature vaporization (PTV) injector and either a 30 m ZB5HT column (i.d. = 0.25 mm, 0.25 µm, Phenomenex, Torrance, CA, USA) or a 60 m DB1 column (i.d. = 0.25 mm, 0.25 µm, Agilent, Santa Clara, CA, USA), ConFlo IV interface, and 253 Plus mass spectrometer (Thermo Scientific).

2.5.4 Data reduction and notation

δ^2H values of individual biphytanes (δ^2H_{BP}) were measured relative to H_2 reference gas (δ^2H_{raw}) and calibrated to the international references scale (VSMOW) using a standard n-alkane mixture (A7, containing C15 through C30 n-alkanes spanning -9 to -263 ‰ vs. VSMOW; A. Schimmelmann, Indiana University). The A7 standard was combined with a C_{36} n-alkane (nC_{36}, -259.2 ‰ vs. VSMOW; A. Schimmelmann, Indiana University) and measured throughout each analytical run at regular intervals and at different concentrations. The BP hydrogen isotope calibration was performed as in Leavitt et al., (2023) using the R packages *isoreader* (v 1.3.0) and *isoprocessor* (v 0.6.11) available at github.com/isoverse (Kopf et al. 2021). In brief, δ^2H_{raw} values were corrected for offset, scale compression and peak-size effects using an inverted multivariate linear regression which was applied to all standards and samples to determine δ^2H_{cal}. Further details of calibration and data reduction are available in Leavitt et al., 2023. The total analytical uncertainty of the corrected δ^2H_{BP} values was calculated using standard error propagation of the peak-size adjusted error estimates and hydrogenation correction assuming all errors to be uncorrelated. The hydrogenation correction ranged from 10.3 to 12.7 ‰ and increased analytical uncertainty by up to 1.9 ‰.

The amplitude of the m/z 2 measurements (i.e. peak amplitudes) are reported in volts (V). All $^2H/^1H$ ratios are reported in delta notation (δ^2H) in permil (‰) units relative to the international seawater

standard on the VSMOW-SLAP (Vienna Standard Mean Ocean Water, Standard Light Antarctic Precipitation) scale.

Eq. (4)

$$\delta^2 H\ (‰) = \left(\frac{{}^2H/{}^1H_{Sample}}{{}^2H/{}^1H_{Standard}} - 1\right) \times 10^3$$

All fractionation factors are reported in epsilon notation ($^2\varepsilon$) in permil (‰) units. The hydrogen isotope fractionation between growth water and BP lipids ($^2\varepsilon_{L/W}$) was calculated as:

Eq. (5 a, b)

$$^2\alpha_{L/W} = \frac{{}^2H/{}^1H_{BP}}{{}^2H/{}^1H_{Water}}$$

$$^2\varepsilon_{L/W}\ (‰) = \left({}^2\alpha_{L/W} - 1\right) \times 10^3$$

Corrected δ^2H_{BP} values and resulting $^2\varepsilon_{L/W}$ fractionation factors from biological replicates (n ≥ 1) and analytical replicates (n ≥ 3 in all cases) were averaged for each experimental condition. All averages are weighted means of individual measurements ($1/\sigma^2$ weights) to account for the amplitude-dependent range in uncertainties. The reported error estimate of each average is the larger of the standard deviation of all replicates or the propagated uncertainty from individual measurements. Abundance weighted averages for δ^2H_{BP} and $^2\varepsilon_{L/W}$ values include all BPs with relative abundance > 5%.

The ring difference (Δε/ring), or changes in $^2\varepsilon_{L/W}$ with increasing number of ring structures were calculated for all pairwise combinations of $^2\varepsilon_{L/W}$ after Leavitt et al., (2023) where X and Y refer to the ring number of BP moieties and X > Y:

Eq. (6)

$$\frac{\Delta\varepsilon}{ring}(‰) = \frac{{}^2\varepsilon_{L/W}(X) - {}^2\varepsilon_{L/W}(Y)}{(X-Y)}$$

Code for all data manipulations and statistical analyses is available on GitHub (https://github.com/carolynnharris/Saci_Enviro_d2H).

3. Results

We examined how temperature, pH, shaking rate, O_2 availability, and electron donor (sucrose) flux influence H-isotope fractionation in *S. acidocaldarius* through a series of batch, fed-batch, and chemostat experiments. Details of the growth responses and lipid iGDGT profile responses to these conditions can be found in Cobban et al., (2020) and Zhou et al., (2019). In brief, each environmental condition independently influences growth rate, the relative abundance of many subsets of iGDGT core lipids, and the RI-GDGT (Cobban et al. 2020; Zhou et al. 2020) (**Table 1, FIG 2A-E, S1**).

Here, we show that each environmental condition also influences the relative abundance of BP lipids and the RI-BP (**Table 2**, **FIG. 2F-O**). Among all samples, the relative abundance of biphytanes

287 averaged 13%, 30%, 49%, 7% for BP-0, -1, -2, and -3, respectively; BP-3 was the least abundant and
288 was not measurable in some samples. RI-BP ranged from 1.01 to 2.04 and, as expected, was
289 positively correlated with RI-GDGT (R^2 = 0.52, *p* = 0.001, **FIG. S2**). Among all samples, the abundance
290 weighted mean δ^2H_{BP} values range from -276 to -225 ‰ and were consistently depleted in ^2H relative
291 to growth water, corresponding to $^2\varepsilon_{L/W}$ values from -230 to -180 ‰, (**Table 2, FIG. 2P-T**).

292 Despite significant effects on growth rate and lipid cyclization, individual environmental parameters
293 had minimal impact on $^2\varepsilon_{L/W}$ values, which spanned a range of 44, 31, 15, 21, and 25 ‰ in the
294 temperature, pH, shaking rate, O_2 availability, and electron donor flux experiments, respectively. We
295 observed a weak linear relationship between environmental conditions and $^2\varepsilon_{L/W}$ only in the electron
296 donor flux experiment, where larger doubling times are associated with slightly less negative $^2\varepsilon_{L/W}$
297 values (smaller offset from water) (R^2 = 0.89, *p* = 0.22, slope = 0.72 ± 0.25 ‰/ hour) (**FIG. 2T**).

298 In the batch and fed-batch experiments, $^2\varepsilon_{L/W}$ values for individual BPs showed no consistent pattern
299 with increasing number of cyclic moieties and the ring difference (Δε/ring) varied widely in direction
300 and magnitude among all treatments (-39 to +24 ‰) (**Table 2**, **FIG. 3A-D, S3A-D**). The variability in
301 mean Δε/ring was smaller, though still not of uniform direction, with values ranging from -5.4 to +10.2
302 ‰ (**Table 2, FIG. S4A-D**). In contrast, $^2\varepsilon_{L/W}$ values in the chemostat experiment generally increased
303 with the number of cyclic moieties, showing offsets of 3.7, 4.1, and 10.1 ‰ for BP-1, BP-2, and BP-3
304 relative to BP-0 (**Table 2, FIG. 3E, S3E**). Similarly, the mean ring difference (Δε/ring) was uniformly
305 positive and showed little variation among doubling times, ranging from 4.9 to 9.2 ‰ (**Table 2, FIG.
306 S4E**). On average in continuous culture, each additional ring contributes a 7.4 ± 2.2 ‰ increase to
307 biphytane $^2\varepsilon_{L/W}$.

308 Correlation matrices show the linear relationship between each environmental condition, growth
309 parameters (doubling time and maximum OD_{600}), mean lipid cyclization indices (RI-BP and RI-GDGT),
310 Δε/ring and abundance weighted $^2\varepsilon_{L/W}$ values for each environmental condition experiment (**FIG. 4**).
311 These plots further demonstrate that the minimal variation in $^2\varepsilon_{L/W}$ observed within each experiment
312 is not related to variation in the experimentally manipulated environmental conditions or any other
313 measured parameter.

314 To explore the possibility that lipid/water fractionation is related to optimal growth, we relate
315 abundance weighted mean $^2\varepsilon_{L/W}$ values to doubling time for each environmental condition (**FIG. 5A-
316 E**). To allow for comparisons among all environmental conditions, we also relate $^2\varepsilon_{L/W}$ to doubling
317 time for all experiments combined. In this pooled dataset, abundance weighted mean $^2\varepsilon_{L/W}$ values
318 range from -230 to -180 ‰ (mean = -204 ± 12 ‰, based on 22 biological replicates; **Table 2**) and
319 showed no correlation to doubling time (**FIG. 5F**, R^2 = 0.0, *p* = 0.97), indicating a decoupling between
320 lipid/water fractionation and growth rate.

4. Discussion

4.1 Archaeal lipid $^{2}\varepsilon_{L/W}$ in response to environmental conditions

The primary goal of this work was to investigate the impact of environmental conditions on lipid/water fractionation in archaeal lipids, which relates to their potential as archives of hydroclimate across space and time. The conditions tested in this study were chosen to encompass the natural conditions of thermoacidophilic archaea, which are globally distributed in hot, acidic features including fumaroles (steam saturated discharges) as geysers and pools in the terrestrial environment, and hydrothermal vents in the marine environment (Lewis et al. 2021). Both realms experience steep gradients in temperature, pH, oxygen, and dissolved solute concentrations, which can change rapidly resulting in disturbed ecological niches (Reysenbach and Cady 2001) leading Archaea to adapt to or evolve strategies to mitigate these challenges (Auernik et al. 2008; Lewis et al. 2021). In. *S. acidocaldarius*, our experimental manipulations of temperature, pH, shaking rate, electron acceptor (O_2) availability, and electron donor (sucrose) flux elicited a 20-fold change in growth rate and 2-fold change in mean biphytane cyclization (RI-BP), but $^{2}\varepsilon_{L/W}$ values were largely invariant (-204 ± 12 ‰, n = 22). This finding is consistent with previous studies that show archaeal lipids are consistently ^{2}H-depleted relative to source water and display a narrow range of $^{2}\varepsilon_{L/W}$ values despite considerable variation in taxonomy, metabolic mode, and growth conditions (Kaneko et al. 2011; Dirghangi and Pagani 2013; Lengger et al. 2020; Wu et al. 2020; Leavitt et al. 2023; Rhim et al. 2024) (**FIG 6**).

In heterotrophic archaea, lipid-bound H can originate from water or the organic substrate used for growth, with intracellular hydride carriers, such as NADPH, mediating the incorporation of H from both sources into lipids (Zhang et al. 2009a; Dirghangi and Pagani 2013; Wijker et al. 2019). In heterotrophs, the NADPH incorporated into lipid products inherits some H from the available organic substrate(s). While there are several potential mechanisms by which each environmental stressor tested here could influence lipid/water fractionation in archaea, our data suggest these processes either do not occur or are insufficient to cause a measurable effect. Temperature, pH, oxygen levels, and nutrient availability are known to trigger physiological responses in archaea, including changes in growth rates, membrane lipid composition, and enzyme activity (Siliakus et al. 2017; Bischof et al. 2019; Cobban et al. 2020). Enzyme kinetics, which are influenced by growth temperature and oxidative stress (Jia et al. 2015), could affect lipid/water fractionation if the enzyme catalyzing hydrogen transfer is associated with a significant isotope effect (Zhang et al. 2009a). High temperatures and low pH reduce water exchange across archaeal membranes to prevent osmotic stress (Siliakus et al. 2017), which could enrich the intracellular water in ^{2}H and potentially reduce apparent lipid/water fractionation (Sachs and Schwab 2011). Additionally, changes in electron donor availability can shift the pathway by which NADPH is reduced, which could influence the δ^{2}H composition of NADPH, which ultimately supplies protons to lipid products. For example, methanogenic archaea switch between the reductive acetyl-CoA and F_{420}-dependent hydrogenase

systems depending on if electron donors (H_2 or formate) are abundant or limiting (Thauer et al. 2008). Despite these possible mechanisms, lipid/water fractionation in *S. acidocaldarius* remains largely invariant in each experiment, indicating that these processes either do not occur or are not significant enough to alter fractionation under the tested conditions. An alternative hypothesis is that *S. acidocaldarius* maintains a constant internal metabolic balance, particularly in NADPH production and utilization, regardless of external conditions.

Physiological responses to stressors impact growth rate and examining $^2\varepsilon_{L/W}$ values in response to optimal vs. suboptimal growth may provide a more coherent explanation for the non-linear patterns we observe across the environmental conditions tested. The $^2\varepsilon_{L/W}$ values for *S. acidocaldarius*, however, are not correlated to growth rate in any single environmental condition experiment or when data for all conditions are pooled. This finding suggesting that cells maintain stable internal metabolic processes resulting in a consistent H-balance over a range of growth rates and is consistent with the theory that a constant $^2\varepsilon_{L/W}$ is a feature of an imperturbable central energy metabolism (Leavitt et al. 2023; Rhim et al. 2024). *S. acidocaldarius*, like most archaea, employs energy-efficient metabolic strategies (Wakagi and Oshima 1987; Liu et al. 2021), possibly as an adaptation to energy-limiting environments (Valentine 2007; Auernik et al. 2008). In tightly controlled metabolic pathways, the balance between supply and use of NADPH reducing power appears to remain constant, even under energy-stress conditions. Previous research suggests archaea may exist in a permanent state of NADPH deficiency such that all NADPH is immediately used for biosynthesis with little to no flux from NADPH back to NADH (Leavitt et al. 2023). It may result that kinetic isotope effects associated with biosynthesis and hydride exchange are not affected by changing growth rates. NADPH deficiency (deemed NADPH flux imbalance by Wijker et al., 2019) is associated with energy limitation, and can provide a framework to relate patterns in $^2\varepsilon_{L/W}$ values to the fluxes of H through dehydrogenase and transhydrogenase enzymes. Indeed, NADPH flux imbalance may explain why all archaea (to-date) and autotrophic and obligately anaerobic bacteria display negative $^2\varepsilon_{L/W}$ values of similar magnitude (Zhang et al. 2009a; Osburn et al. 2016; Wijker et al. 2019; Rhim et al. 2024). This similarity is striking given that fatty acids and isoprenoid GDGTs are formed via different biosynthetic pathways and suggests that the ultimate control on $^2\varepsilon_{L/W}$ values may be related to free energy yields (Rhim et al. 2024).

Both the O_2 availability and sucrose flux experiments test the hypothesis that energy limitation – either terminal electron acceptor or donor – can alter $^2\varepsilon_{L/W}$ values in archaea. These experiments produced the largest range in doubling times (2 to 50 hours and 7 to 44 hours in the O_2 availability and electron donor experiments, respectively); yet $^2\varepsilon_{L/W}$ values remained consistently negative (-217 to -196 ‰ and -276 to -244 ‰, respectively). *N. maritimus* is the only other archaeon in which the relationship between electron donor (ammonium) flux and lipid/water fractionation was examined (Leavitt et al. 2023). *N. maritimus* similarly exhibited no significant correlation between a three-fold change in doubling time and $^2\varepsilon_{L/W}$ (R^2 = 0.22, p = 0.07, slope = 0.18 ± 0.09 ‰/ hour) (Leavitt et al. 2023). The authors speculate this strain maintains a consistent H-balance over a range of electron

donor fluxes as an adaptation that allows cells to perform nitrification with energy-efficient CO_2 fixation in oligotrophic environments (Leavitt et al. 2023). These findings suggest that archaea with diverse physiologies (e.g., heterotrophy vs. chemoautotrophy, extremophily vs. mesophily) maintain a consistent lipid-to-water fractionation that is minimally affected by free energy availability and may reflect the fact that Archaea are adapted to chronic energy limitation (Valentine 2007; Auernik et al. 2008). This stability may reflect tightly regulated physiological processes, such as isoenzyme switching and modulation of enzyme activities, which help maintain metabolic homeostasis under both optimal and sub-optimal growth conditions (Bräsen et al. 2014). In contrast, in bacteria and some planktonic eukaryotes faster growth is associated with larger lipid/water fractionation (Schouten et al. 2006; Zhang et al. 2009b; Sachs and Schwab 2011) and $^{2}\varepsilon_{L/W}$ values for Bacteria are influenced by electron donor flux (Zhang et al. 2009a; Osburn et al. 2016; Wijker et al. 2019).

The only other study in archaea to examine the relationship between environmental conditions and $^{2}\varepsilon_{L/W}$ cultured the halophilic heterotrophic archaeon, *H. marismortui* (which produces archaeol diethers), under varying temperatures and salinities when grown on complex rich medium (Dirghangi and Pagani 2013). The resulting $^{2}\varepsilon_{Archaeol/W}$ values are relatively invariant (ranging from -126 to -143 ‰; more enriched than our observations for *S. acidocaldarius*) and are decoupled from growth rate (**FIG. S5;** R^2 = 0.07, p = 0.7, slope = 0.85 ± 1.84 ‰ / hour; Dirghangi and Pagani 2013), providing more evidence that archaea maintain a stable internal H-balance across a range of growth conditions.

The impact of growth phase on H-isotope dynamics has not been studied in depth. The batch and fed-batch experiment techniques used here for *S. acidocaldarius* and in the *H. marismortui* study integrate across growth stages, whereas the chemostat electron donor flux experiments for *S. acidocaldarius* and *N. maritimus* achieve constant growth rates. A recent study grew *A. fulgidus* in batch cultures and found that $^{2}\varepsilon_{L/W}$ values were more depleted (larger offset from water) during exponential phase relative to stationary phase (Rhim et al. 2024). This pattern was consistent between heterotrophic and autotrophic experiments. The culture conditions in Rhim et al. resulted in a threefold difference in growth rates (similar change to the *N. maritimus* study, but much smaller range than the 20-fold change we report for *S. acidocaldarius* here) and a 50 ‰ change in $^{2}\varepsilon_{L/W}$ values (-280 ‰ to -230 ‰). Rhim and coauthors conclude that both metabolic mode (heterotrophic vs. autotrophic growth) and growth phase impact $^{2}\varepsilon_{L/W}$ values, though the total variance among all treatments was small and overlaps which ranges reported for other archaea (Rhim et al. 2024).

4.2 Effect of biphytane ring number on $^{2}\varepsilon_{L/W}$

Stoichiometric modeling predicts that BPs with more rings incorporate less of the highly-fractionated hydrogen donated through GGR reduction, a process where the enzyme geranyl-geranyl reductase (GGR) catalyzes the reduction of double bonds in isoprenoid chains, thereby affecting the isotopic composition of the resulting lipids (Leavitt et al. 2023). Interestingly, in our *S. acidocaldarius* work, this stepwise enrichment is only seen in the chemostat experiments, where each additional ring contributes 7.4 ± 2.2 ‰ to biphytane $^{2}\varepsilon_{L/W}$ values. In the batch and fed-batch experiments, there

is no consistent dependence of $^{2}\varepsilon_{L/W}$ values on the number of biphytane moieties. iGDGT-derived BPs extracted from marine sediments also lack a clear stepwise enrichment with increasing ring moieties (Kaneko et al. 2011), but this likely occurs because sediments integrate lipids synthesized by different populations of archaea that are either growing on multiple substrates or in different water masses (Kaneko et al. 2011),. It is less clear why the pure *S. acidocaldarius* batch and fed-batch cultures do not display a ring-specific pattern, though it perhaps relates to variations in biosynthetic fractionations accompanying changes in lipid biosynthesis across the growth phases (Elling et al. 2014).

Considering all the available data, this enrichment pattern appears only minimally affected by differences in growth rate and metabolism, as the magnitude of per-ring increase in $^{2}\varepsilon_{L/W}$ value is similar for *Sulfolobus* sp. (Kaneko et al. 2011), *S. acidocaldarius* (chemostat experiment in this study), and *N. maritimus* (Leavitt et al. 2023), which collectively represent a 5-fold range of growth rates, and a variety of metabolisms and carbon substrates (*Sulfolobus* sp. = yeast extract + O_2; *S. acidocaldarius* = sucrose + O_2; *N. maritimus* = chemoautotroph on NH_4 + O_2). The magnitude of this stepwise enrichment, however, is small and would likely have a minor impact (usually < 10 ‰) on the abundance weighted mean $^{2}\varepsilon_{L/W}$ value even in cases where the BP Ring Index was markedly different among samples (Leavitt et al. 2023).

4.3 Archaeal lipid $^{2}\varepsilon_{L/W}$ as a function of central metabolism

The *S. acidocaldarius* $^{2}\varepsilon_{L/W}$ values we report are broadly similar to results from previous experimental investigations of the *Sulfolobus* genus cultured heterotrophically. When grown at 75 °C and pH 2 on yeast extract, a *Sulfolobus* strain displayed $^{2}\varepsilon_{L/W}$ values from -213 to -161 ‰ for BP-0 to -4 (abundance weighted mean = -180 ‰ (Kaneko et al. 2011) vs. -204 ± 12 ‰ for *S. acidocaldarius* here). In another study, *Sulfolobus solfataricus* grown at 76 °C and pH 3.5 on glutamate displayed more enriched $^{2}\varepsilon_{L/W}$ values, averaging -134 ‰ when intact iGDGT-1 and -2 were analyzed (Lengger et al. 2020). The difference in $^{2}\varepsilon_{L/W}$ values may in part be due to the structures analyzed. Lengger and colleagues analyzed intact iGDGTs including the glycerols which may enrich the $\delta^{2}H_{iGDGT}$ composition, though the different substrate may also play a role (Lengger et al. 2020). Glutamate, an amino acid, is a more complex substrate than simple sugars (such as sucrose) and primarily enters the *Sulfolobus* central metabolism through the TCA cycle (Quehenberger et al. 2019). Simple sugars enter metabolism primarily through the Entner-Doudoroff pathway, which converts the sugar to intermediates that feed into the TCA cycle (Quehenberger et al. 2019).

When *S. acidocaldarius* is grown heterotrophically on a simple sugar (glucose), the weighted mean $\delta^{2}H$ composition of biphytane lipids is strongly correlated with $\delta^{2}H_{Water}$, indicating a strong first-order control (see *Supplementary Materials*, **Fig. S6**). A simple Isotope mass balance model (**Eq. S1**) suggests water contributes at least 56 ± 1% of the total H flux to lipids (**FIG. S7**). Further experimental

work and complementary isotope flux models are needed to determine the specific pathways (and associated isotope effects) used during iGDGT synthesis in *S. acidocaldarius* (Harris et al. 2022).

Autotrophic archaea that produce iGDGTs, however, source their entire H budget to lipids from water in the growth environment and show more negative $^{2}\varepsilon_{L/W}$ values than we observe for *S. acidocaldarius*. In the marine chemoautotroph, *N. maritimus*, grown in continuous culture, BP/water fractionation ranged from -272 to -260 ‰ (Leavitt et al. 2023). Similarly, BP/water fractionations for a metabolically-flexible archaeon, *Archaeoglobus fulgidus*, ranged from -280 to -226 ‰ when cultured with several unique carbon substrates and electron donor/acceptor pairs (Rhim et al. 2024). This difference may be driven by the distinct metabolic modes used (e.g., autotrophy vs. heterotrophy) and/or by unique metabolic pathways that employ various intracellular hydride carriers and reductants to bring H's to the lipid sites, which could generate different net biosynthetic fractionations. Metabolic flux models suggest that in autotrophic archaea (e.g., *N. maritimus*), H-isotope fractionation due to the electron transport chain and NADPH generation result in more depleted lipids than for heterotrophic archaea, such as *Sulfolobus* species, because the source of NADPH impacts $^{2}\varepsilon_{L/W}$ values (Leavitt et al. 2023). In both heterotrophic and aerobic archaea, most NADPH is generated by glucose dehydrogenase and potentially glyceraldehyde dehydrogenase from the Entner-Doudoroff pathway (Nunn et al. 2010; Bräsen et al. 2014).

Overall, the range of $^{2}\varepsilon_{L/W}$ values in Archaeal lipids is much narrower than the ranges observed in Bacteria or Eukarya (**FIG. 6**). Reported $^{2}\varepsilon_{L/W}$ values for bacterial fatty acids vary over 600 ‰ and include large negative and large positive values (Campbell et al. 2009; Zhang et al. 2009a; Osburn et al. 2016; Wijker et al. 2019; Rhim et al. 2024). In Eukarya, $^{2}\varepsilon_{L/W}$ values are uniformly negative and span over 300 ‰, though certain lipid classes group together (Sessions et al. 1999; Zhang and Sachs 2007; Sachs et al. 2016). Lipids that are formed via the same biosynthetic pathway (e.g., acetogenic or isoprenoid pathway) tend to occupy distinct ranges of $^{2}\varepsilon_{L/W}$ (Rhim et al. 2024). Isoprenoid lipids produced via the MVA pathway in eukaryotes have similar $^{2}\varepsilon_{L/W}$ values to iGDGT-derived biphytanes in archaea (Rhim et al. 2024). This similarity suggests that the MVA pathway used for isoprenoid lipid biosynthesis has a large net fractionation in both domains of life.

4.4 Applications and Conclusion

Our calibration of biphytane $\delta^{2}H$ as a proxy water $\delta^{2}H$ in *S. acidocaldarius* has significant implications for paleohydroclimate and paleoecology reconstructions. First, this calibration potentially allows hydroclimate factors like precipitation, elevation, and seasonality to be reconstructed for environments that do not contain traditionally analyzed lipid biomarkers (e.g., plant waxes) – this includes extreme environments that do not support plant growth (e.g., hydrothermal systems, hypersaline salars, etc.). Archaeal lipid $\delta^{2}H$ will be most powerful as a proxy in cases where a single-substrate source is a reasonable assumption.

Second, biphytane δ^2H could be applied to marine or lacustrine sedimentary archives where multiple sources of organic matter are suspected, such as a mix of plant waxes representing *in situ* marine/ aquatic production and allochthonous terrestrial production (e.g., aeolian deposition). In this case, plant wax δ^2H would reflect a mixture of growth waters (marine/lake water and soil water). In contrast, iGDGTs are likely derived solely from archaea living in the overlying water column with few potential terrestrial sources and thus their δ^2H composition would only reflect marine/lake water (Pearson and Ingalls 2013).

Here, we show that in the model thermoacidophile *S. acidocaldarius* grown on simple sugars, lipid-water fractionation ($^2\varepsilon_{L/W}$) is not dependent on any of the environmental conditions tested or on growth rate. This finding suggests that *S. acidocaldarius* may have evolved stable metabolisms that exist in a constant NADPH deficit, possibly reflecting adaptation to energy-limiting environments. We conclude that *S. acidocaldarius* will likely demonstrate reliably invariant lipid/water fractionation regardless of growth rate, nutrient status, or energy availability, and that the environmental expression of archaeal $^2\varepsilon_{L/W}$ may be more constant than for marine algae. This calibration underscores the potential for archaeal lipid δ^2H as a proxy for past hydroclimates that could complement or be used independently of eukaryotic lipid δ^2H. Future research should focus on exploring the effects of growth phase and metabolic pathways on lipid/water fractionation in *S. acidocaldarius* and other archaeal species. Expanding these investigations to include more diverse environmental conditions, such as varying carbon substrates or mixed microbial communities, could further validate the consistency of $^2\varepsilon_{L/W}$ and refine its utility as a hydrological proxy. Additionally, integrating isotope flux models with experimental data may help elucidate the specific biochemical pathways responsible for the observed fractionation patterns (Harris et al. 2022).

Acknowledgements

This research was supported by research grant NSF EAR #1928303940 (WDL, SHK); Simons Foundation Award #623881 (WDL); Dartmouth College (WDL); National Aeronautics and Space Administration (NASA) New Hampshire Space Grant (NASA-SSW-80NSSC19K0539); Deutsche Forschungsge-meinschaft grant 441217575 (F.J.E.). The authors thank the CU Boulder Earth Systems Stable Isotope Lab (CUBES-SIL) Core Facility (RRID:SCR_019300) for analytical contributions; B. Chiu (then at Dartmouth), J. Blewett (then at Harvard), S. Carter (Harvard), H. Batther (CU Boulder) and A. Maloney (CU Boulder) for expert laboratory support; Simon D. Kelly from International Atomic Energy Agency, Vienna for measuring the δ^2H composition of carbon substrates; and all members of the Leavitt lab for all their support.

536 **References**

537 Abrahim A, Cannavan A, Kelly SD (2020) Stable isotope analysis of non-exchangeable hydrogen in
538 carbohydrates derivatised with N-methyl-bis-trifluoroacetamide by gas chromatography –
539 Chromium silver reduction/High temperature Conversion-isotope ratio mass spectrometry
540 (GC-CrAg/HTC-IRMS). Food Chemistry 318:126413.
541 https://doi.org/10.1016/j.foodchem.2020.126413

542 Auernik KS, Cooper CR, Kelly RM (2008) Life in hot acid: pathway analyses in extremely
543 thermoacidophilic archaea. Current Opinion in Biotechnology 19:445–453.
544 https://doi.org/10.1016/j.copbio.2008.08.001

545 Bender, Suess, Chitwood, Bradley (2016) Investigating genetic loci that encode plant-derived
546 paleoclimate proxies. pp PP24B-03

547 Bischof LF, Haurat MF, Hoffmann L, et al (2019) Early Response of Sulfolobus acidocaldarius to
548 Nutrient Limitation. Front Microbiol 9:3201. https://doi.org/10.3389/fmicb.2018.03201

549 Bräsen C, Esser D, Rauch B, Siebers B (2014) Carbohydrate Metabolism in Archaea: Current
550 Insights into Unusual Enzymes and Pathways and Their Regulation. Microbiol Mol Biol Rev
551 78:89–175. https://doi.org/10.1128/MMBR.00041-13

552 Campbell BJ, Li C, Sessions AL, Valentine DL (2009) Hydrogen isotopic fractionation in lipid
553 biosynthesis by H2-consuming Desulfobacterium autotrophicum. Geochimica et
554 Cosmochimica Acta 73:2744–2757. https://doi.org/10.1016/j.gca.2009.02.034

555 Cobban A, Zhang Y, Zhou A, et al (2020) Multiple environmental parameters impact core lipid
556 cyclization in Sulfolobus acidocaldarius. Environmental Microbiology 1–28

557 Dawson D, Grice K, Wang SX, et al (2004) Stable hydrogen isotopic composition of hydrocarbons in
558 torbanites (Late Carboniferous to Late Permian) deposited under various climatic
559 conditions. Organic Geochemistry 35:189–197.
560 https://doi.org/10.1016/j.orggeochem.2003.09.004

561 Dawson KS, Osburn MR, Sessions AL, Orphan VJ (2015) Metabolic associations with archaea drive
562 shifts in hydrogen isotope fractionation in sulfate-reducing bacterial lipids in cocultures
563 and methane seeps. Geobiology 13:462–477. https://doi.org/10.1111/gbi.12140

564 De Rosa M, Gambacorta A (1988) The lipids of archaebacteria. Progress in Lipid Research 27:153–
565 175. https://doi.org/10.1016/0163-7827(88)90011-2

566 Dirghangi SS, Pagani M (2013) Hydrogen isotope fractionation during lipid biosynthesis by
567 Haloarcula marismortui. Geochimica et Cosmochimica Acta 119:381–390.
568 https://doi.org/10.1016/j.gca.2013.05.023

569 Elling FJ, Könneke M, Lipp JS, et al (2014) Effects of growth phase on the membrane lipid
570 composition of the thaumarchaeon Nitrosopumilus maritimus and their implications for
571 archaeal lipid distributions in the marine environment. Geochimica et Cosmochimica Acta
572 141:579–597. https://doi.org/10.1016/j.gca.2014.07.005

Elling FJ, Könneke M, Nicol GW, et al (2017) Chemotaxonomic characterisation of the thaumarchaeal lipidome. Environmental Microbiology 19:2681–2700. https://doi.org/10.1111/1462-2920.13759

Gat JR (1996) Oxygen and hydrogen isotopes in the hydrologic cycle. Annual Review of Earth and Planetary Sciences 24:225–262. https://doi.org/10.1146/annurev.earth.24.1.225

Harris C, Rhim J, Zhang Y, et al (2022) Determining controls on hydrogen isotope fractionation in archaeal tetraether lipids in a thermoacidophilic archaeal heterotroph. In: Goldschmidt2022 abstracts. European Association of Geochemistry, Honolulu, HI, USA

Hayes JM (2001) Fractionation of carbon and hydrogen isotopes in biosynthetic processes. Stable Isotope Geochemistry 43:225–277. https://doi.org/10.2138/gsrmg.43.1.225

Hurley SJ, Elling FJ, Könneke M, et al (2016) Influence of ammonia oxidation rate on thaumarchaeal lipid composition and the TEX86 temperature proxy. Proceedings of the National Academy of Sciences of the United States of America 113:7762–7767. https://doi.org/10.1073/pnas.1518534113

Jia B, Liu J, Van Duyet L, et al (2015) Proteome profiling of heat, oxidative, and salt stress responses in Thermococcus kodakarensis KOD1. Front Microbiol 6:. https://doi.org/10.3389/fmicb.2015.00605

Kaneko M, Kitajima F, Naraoka H (2011) Stable hydrogen isotope measurement of archaeal ether-bound hydrocarbons. Organic Geochemistry 42:166–172. https://doi.org/10.1016/j.orggeochem.2010.11.002

Kopec BG, Feng X, Posmentier ES, et al (2018) Use of principal component analysis to extract environmental information from lake water isotopic compositions. Limnology & Oceanography 63:1340–1354. https://doi.org/10.1002/lno.10776

Kopf S, Davidheiser-Kroll B, Kocken I (2021) Isoreader: An R package to read stable isotope data files for reproducible research. JOSS 6:2878. https://doi.org/10.21105/joss.02878

Ladd SN, Nelson DB, Bamberger I, et al (2021) Metabolic exchange between pathways for isoprenoid synthesis and implications for biosynthetic hydrogen isotope fractionation. New Phytologist 231:1708–1719. https://doi.org/10.1111/nph.17510

Leavitt WD (2016) The Inner Lives of Archaea: the hydrogen isotopic composition of Archaeal lipids as a proxy of metabolic state

Leavitt WD, Kopf SH, Weber Y, et al (2023) Controls on the hydrogen isotope composition of tetraether lipids in an autotrophic ammonia-oxidizing marine archaeon. Geochimica et Cosmochimica Acta 352:194–210. https://doi.org/10.1016/j.gca.2023.04.033

Leavitt WD, Murphy SJL, Lynd LR, Bradley AS (2017) Hydrogen isotope composition of Thermoanaerobacterium saccharolyticum lipids: Comparing wild type with a nfn-transhydrogenase mutant. Organic Geochemistry 113:239–241. https://doi.org/10.1016/j.orggeochem.2017.06.020

610 Lengger SK, Weber Y, Taylor KWR, et al (2020) Determination of the d2H values of high molecular
611 weight lipids by high temperature GC coupled to isotope ratio mass spectro. Rapid
612 Communications in Mass Spectrometry

613 Lewis AM, Recalde A, Bräsen C, et al (2021) The biology of thermoacidophilic archaea from the
614 order Sulfolobales. FEMS Microbiology Reviews 1–60.
615 https://doi.org/10.1093/femsre/fuaa063

616 Liu J, An Z (2019) Variations in hydrogen isotopic fractionation in higher plants and sediments
617 across different latitudes: Implications for paleohydrological reconstruction. Science of
618 The Total Environment 650:470–478. https://doi.org/10.1016/j.scitotenv.2018.09.047

619 Liu L-J, Jiang Z, Wang P, et al (2021) Physiology, Taxonomy, and Sulfur Metabolism of the
620 Sulfolobales, an Order of Thermoacidophilic Archaea. Front Microbiol 12:768283.
621 https://doi.org/10.3389/fmicb.2021.768283

622 Love GD, Zumberge JA (2021) Emerging Patterns in Proterozoic Lipid Biomarker Records, 1st edn.
623 Cambridge University Press

624 Maloney AE, Shinneman ALC, Hemeon K, Sachs JP (2016) Exploring lipid 2H/1H fractionation
625 mechanisms in response to salinity with continuous cultures of the diatom Thalassiosira
626 pseudonana. Organic Geochemistry 101:154–165.
627 https://doi.org/10.1016/j.orggeochem.2016.08.015

628 McFarlin JM, Axford Y, Masterson AL, Osburn MR (2019) Calibration of modern sedimentary δ2H
629 plant wax-water relationships in Greenland lakes. Quaternary Science Reviews
630 225:105978. https://doi.org/10.1016/j.quascirev.2019.105978

631 Nunn CEM, Johnsen U, Schönheit P, et al (2010) Metabolism of Pentose Sugars in the
632 Hyperthermophilic Archaea Sulfolobus solfataricus and Sulfolobus acidocaldarius. Journal
633 of Biological Chemistry 285:33701–33709. https://doi.org/10.1074/jbc.M110.146332

634 Osburn MR, Dawson KS, Fogel ML, Sessions AL (2016) Fractionation of hydrogen isotopes by
635 sulfate- and nitrate-reducing bacteria. Frontiers in Microbiology 7:1–16.
636 https://doi.org/10.3389/fmicb.2016.01166

637 Osburn MR, Sessions AL, Pepe-Ranney C, Spear JR (2011) Hydrogen-isotopic variability in fatty
638 acids from Yellowstone National Park hot spring microbial communities. Geochimica et
639 Cosmochimica Acta 75:4830–4845. https://doi.org/10.1016/j.gca.2011.05.038

640 Pearson A, Ingalls AE (2013) Assessing the use of archaeal lipids as marine environmental proxies.
641 Annual Review of Earth and Planetary Sciences 41:359–384.
642 https://doi.org/10.1146/annurev-earth-050212-123947

643 Quehenberger J, Albersmeier A, Glatzel H, et al (2019) A defined cultivation medium for Sulfolobus
644 acidocaldarius. Journal of Biotechnology 301:56–67.
645 https://doi.org/10.1016/j.jbiotec.2019.04.028

Quehenberger J, Pittenauer E, Allmaier G, Spadiut O (2020) The influence of the specific growth rate on the lipid composition of Sulfolobus acidocaldarius. Extremophiles 24:413–420. https://doi.org/10.1007/s00792-020-01165-1

Reysenbach A-L, Cady SL (2001) Microbiology of ancient and modern hydrothermal systems. Trends in Microbiology 9:79–86. https://doi.org/10.1016/S0966-842X(00)01921-1

Rhim JH, Zhou A, Amenabar MJ, et al (2024) Mode of carbon and energy metabolism shifts lipid composition in the thermoacidophile *Acidianus*. Appl Environ Microbiol e01369-23. https://doi.org/10.1128/aem.01369-23

Sachs J (2014) Hydrogen Isotope Signatures in the Lipids of Phytoplankton. In: Treatise on Geochemistry. Elsevier, pp 79–94

Sachs JP, Kawka OE (2015) The influence of growth rate on 2H/1H fractionation in continuous cultures of the coccolithophorid Emiliania huxleyi and the diatom Thalassiosira pseudonana. PLoS ONE 10:1–27. https://doi.org/10.1371/journal.pone.0141643

Sachs JP, Maloney AE, Gregersen J (2017) Effect of light on 2H/1H fractionation in lipids from continuous cultures of the diatom Thalassiosira pseudonana. Geochimica et Cosmochimica Acta 209:204–215. https://doi.org/10.1016/j.gca.2017.04.008

Sachs JP, Maloney AE, Gregersen J, Paschall C (2016) Effect of salinity on 2H/1H fractionation in lipids from continuous cultures of the coccolithophorid Emiliania huxleyi. Geochimica et Cosmochimica Acta 189:96–109. https://doi.org/10.1016/j.gca.2016.05.041

Sachs JP, Schwab VF (2011) Hydrogen isotopes in dinosterol from the Chesapeake Bay estuary. Geochimica et Cosmochimica Acta 75:444–459. https://doi.org/10.1016/j.gca.2010.10.013

Sachse D, Billault I, Bowen GJ, et al (2012) Molecular paleohydrology: Interpreting the hydrogen-isotopic composition of lipid biomarkers from photosynthesizing organisms. Annual Review of Earth and Planetary Sciences 40:221–249. https://doi.org/10.1146/annurev-earth-042711-105535

Schouten S, Hopmans EC, SchefuB E, Sinninghe Damsté JS (2002) Distributional variations in marine crenarchaeotal membrane lipids: a new tool for reconstructing ancient sea water temperatures? Earth and Planetary Science Letters 265–274. https://doi.org/10.5642/aliso.19881201.09

Schouten S, Hopmans EC, Sinninghe Damsté JS (2013) The organic geochemistry of glycerol dialkyl glycerol tetraether lipids: A review. Organic Geochemistry 54:19–61. https://doi.org/10.1016/j.orggeochem.2012.09.006

Schouten S, Ossebaar J, Schreiber K, et al (2006) The effect of temperature, salinity and growth rate on the stable hydrogen isotopic composition of long chain alkenones produced by Emiliania huxleyi and Gephyrocapsa oceanica. Biogeosciences 3:113–119. https://doi.org/10.5194/bg-3-113-2006

682 Sessions AL (2016) Factors controlling the deuterium contents of sedimentary hydrocarbons.
683 Organic Geochemistry 96:43–64. https://doi.org/10.1016/j.orggeochem.2016.02.012

684 Sessions AL, Burgoyne TW, Schimmelmann A, Hayes JM (1999) Fractionation of hydrogen isotopes
685 in lipid biosynthesis. Organic Geochemistry 30:1193–1200. https://doi.org/10.1016/S0146-
686 6380(99)00094-7

687 Sessions AL, Jahnke LL, Schimmelmann A, Hayes JM (2002) Hydrogen isotope fractionation in
688 lipids of the methane-oxidizing bacterium Methylococcus capsulatus. Geochimica et
689 Cosmochimica Acta 66:3955–3969. https://doi.org/10.1016/S0016-7037(02)00981-X

690 Sessions AL, Sylva SP, Summons RE, Hayes JM (2004) Isotopic exchange of carbon-bound
691 hydrogen over geologic timescales. Geochimica et Cosmochimica Acta 68:1545–1559.
692 https://doi.org/10.1016/j.gca.2003.06.004

693 Siliakus MF, Van Der Oost J, Kengen SWM (2017) Adaptations of archaeal and bacterial membranes
694 to variations in temperature, pH and pressure. Extremophiles 21:651–670.
695 https://doi.org/10.1007/s00792-017-0939-x

696 Thauer RK, Kaster A-K, Seedorf H, et al (2008) Methanogenic archaea: ecologically relevant
697 differences in energy conservation. Nat Rev Microbiol 6:579–591.
698 https://doi.org/10.1038/nrmicro1931

699 Torres-Romero I, Zhang H, Wijker RS, et al (2024) Hydrogen isotope fractionation is controlled by
700 CO_2 in coccolithophore lipids. Proc Natl Acad Sci USA 121:e2318570121.
701 https://doi.org/10.1073/pnas.2318570121

702 Valentine DL (2009) Isotopic remembrance of metabolism past. Proceedings of the National
703 Academy of Sciences of the United States of America 106:12565–12566.
704 https://doi.org/10.1073/pnas.0906428106

705 Valentine DL (2007) Adaptations to energy stress dictate the ecology and evolution of the Archaea.
706 Nature Reviews Microbiology 5:316–323. https://doi.org/10.1038/nrmicro1619

707 Van de Vossenberg JLCM, Driessen AJM, Konings WN (1998) The essence of being extremophilic:
708 The role of the unique archaeal membrane lipids. Extremophiles 2:163–170.
709 https://doi.org/10.1007/s007920050056

710 Van Der Meer MTJ, Benthien A, French KL, et al (2015) Large effect of irradiance on hydrogen
711 isotope fractionation of alkenones in Emiliania huxleyi. Geochimica et Cosmochimica Acta
712 160:16–24. https://doi.org/10.1016/j.gca.2015.03.024

713 Wagner M, Van Wolferen M, Wagner A, et al (2012) Versatile Genetic Tool Box for the
714 Crenarchaeote Sulfolobus acidocaldarius. Front Microbio 3:.
715 https://doi.org/10.3389/fmicb.2012.00214

716 Wakagi T, Oshima T (1987) Energy metabolism of a thermoacidophilic archaebacterium,Sulfolobus
717 acidocaldarius. Origins Life Evol Biosphere 17:391–399.
718 https://doi.org/10.1007/BF02386477

Wijker RS, Sessions AL, Fuhrer T, Phan M (2019) 2H/1H variation in microbial lipids is controlled by NADPH metabolism. Proceedings of the National Academy of Sciences of the United States of America 116:12173–12182. https://doi.org/10.1073/pnas.1818372116

Wolfshorndl M, Danford R, Sachs JP (2019) 2H/1H fractionation in microalgal lipids from the North Pacific Ocean: Growth rate and irradiance effects. Geochimica et Cosmochimica Acta 246:317–338. https://doi.org/10.1016/j.gca.2018.11.027

Wu W, Meador TB, Könneke M, et al (2020) Substrate-dependent incorporation of carbon and hydrogen for lipid biosynthesis by Methanosarcina barkeri. Environmental Microbiology Reports. https://doi.org/10.1111/1758-2229.12876

Yang W, Chen H, Chen Y, et al (2023) Thermophilic archaeon orchestrates temporal expression of GDGT ring synthases in response to temperature and acidity stress. Environmental Microbiology 25:575–587. https://doi.org/10.1111/1462-2920.16301

Zhang X, Gillespie AL, Sessions AL (2009a) Large D/H variations in bacterial lipids reflect central metabolic pathways. Proceedings of the National Academy of Sciences of the United States of America 106:12580–12586. https://doi.org/10.1073/pnas.0903030106

Zhang YG, Pagani M, Wang Z (2016) Ring Index: A new strategy to evaluate the integrity of TEX_{86} paleothermometry. Paleoceanography 31:220–232. https://doi.org/10.1002/2015PA002848

Zhang Z, Sachs JP (2007) Hydrogen isotope fractionation in freshwater algae: I. Variations among lipids and species. Organic Geochemistry 38:582–608. https://doi.org/10.1016/j.orggeochem.2006.12.004

Zhang Z, Sachs JP, Marchetti A (2009b) Hydrogen isotope fractionation in freshwater and marine algae: II. Temperature and nitrogen limited growth rate effects. Organic Geochemistry 40:428–439. https://doi.org/10.1016/j.orggeochem.2008.11.002

Zhou A, Weber Y, Chiu BK, et al (2020) Energy flux controls tetraether lipid cyclization in Sulfolobus acidocaldarius. Environmental Microbiology 22:343–353. https://doi.org/10.1111/1462-2920.14851

Tables

Table 1. Summary of culture conditions and descriptive growth statistics for *S. acidocaldarius* grown under varying environmental conditions. Data for batch and fed-batch environmental condition experiments were initially reported in Cobban et al., (2020), data for chemostat experiment was initially reported in Zhou et al., (2019).

Table 2. Descriptive statistics for biphytanyl (BP) lipids derived from iGDGTs for *S. acidocaldarius* grown under varying environmental conditions. Mean and sd include biological replication and technical replication (multiple injections). *N* = number of biological replicates in each treatment, *n* is the number of replicates analyzed for lipid composition. *For batch experiments, RPM is shaking rate; for bioreactor experiments, RPM is impellor speed.

Figures

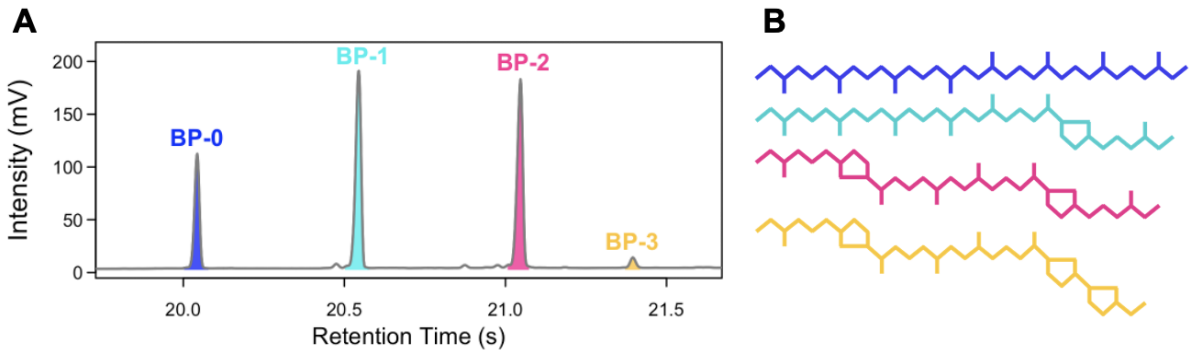

Fig 1. (A) Representative chromatogram of intensity vs. retention time for four iGDGT-derived biphytane (BP) moieties identified in *S. acidocaldarius* biomass that are named for the number of cyclopentane rings they contain. Although a BP-3 peak was detected, in many cases it is present in too low quantities to perform isotopic measurements **(B)** The identity and structure of BP-0 to BP-3.

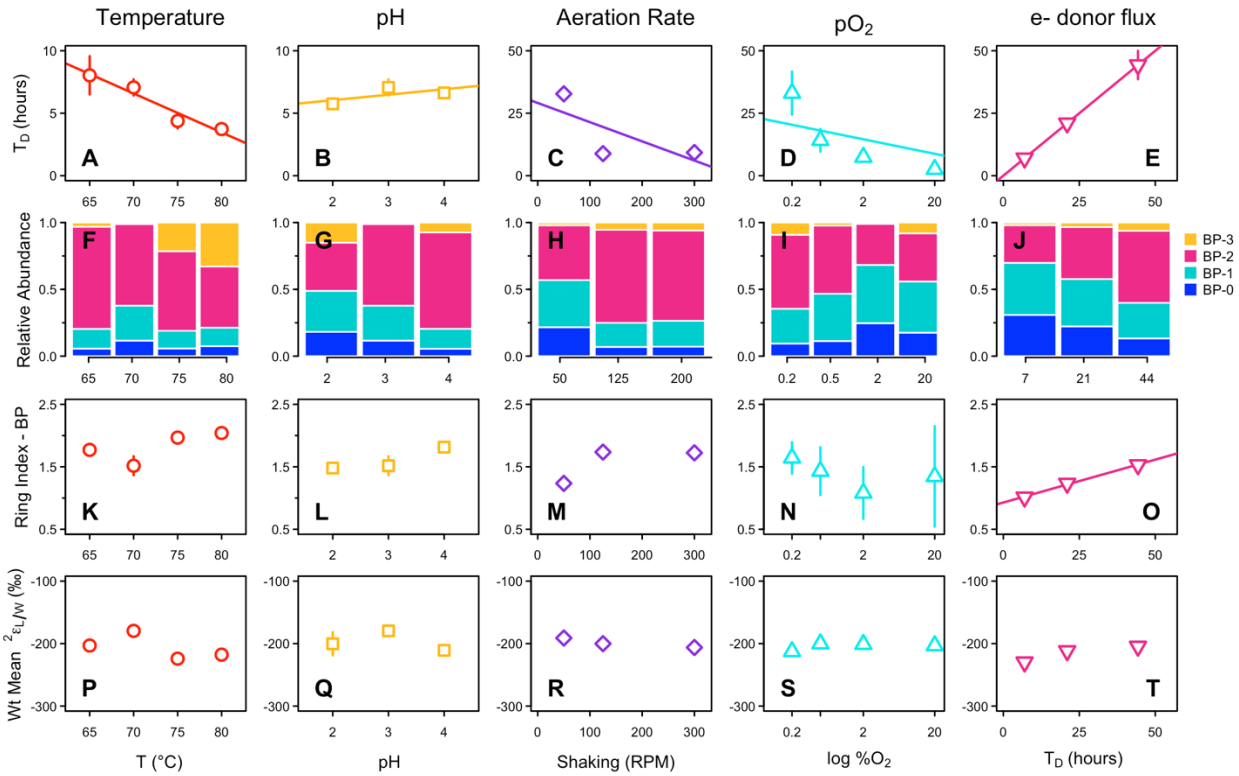

Fig. 2. Results for *S. acidocaldarius* grown under varying environmental conditions. Top row (**A-E**): Doubling time in response to each environmental condition. Second row (**F-J**): Relative abundance of biphytane (BP) lipids derived from iGDGTs. BP-3 was the least abundant and was below the detection limit in some samples. Bars represent the mean across replicates for each treatment level. Third row (**K-O**): Ring Index (RI-BP) of biphytane lipids derived from iGDGTs. Bottom row (**P-T**) The abundance weighted mean H-isotope fractionation ($^{2}\varepsilon_{L/W}$) between growth water and biphytanes. For all rows, points represent the mean and propagated error across biological and technical replicates for each treatment level. In many cases, error bars are smaller than symbols. Only statistically significant regressions are shown ($p < 0.05$).

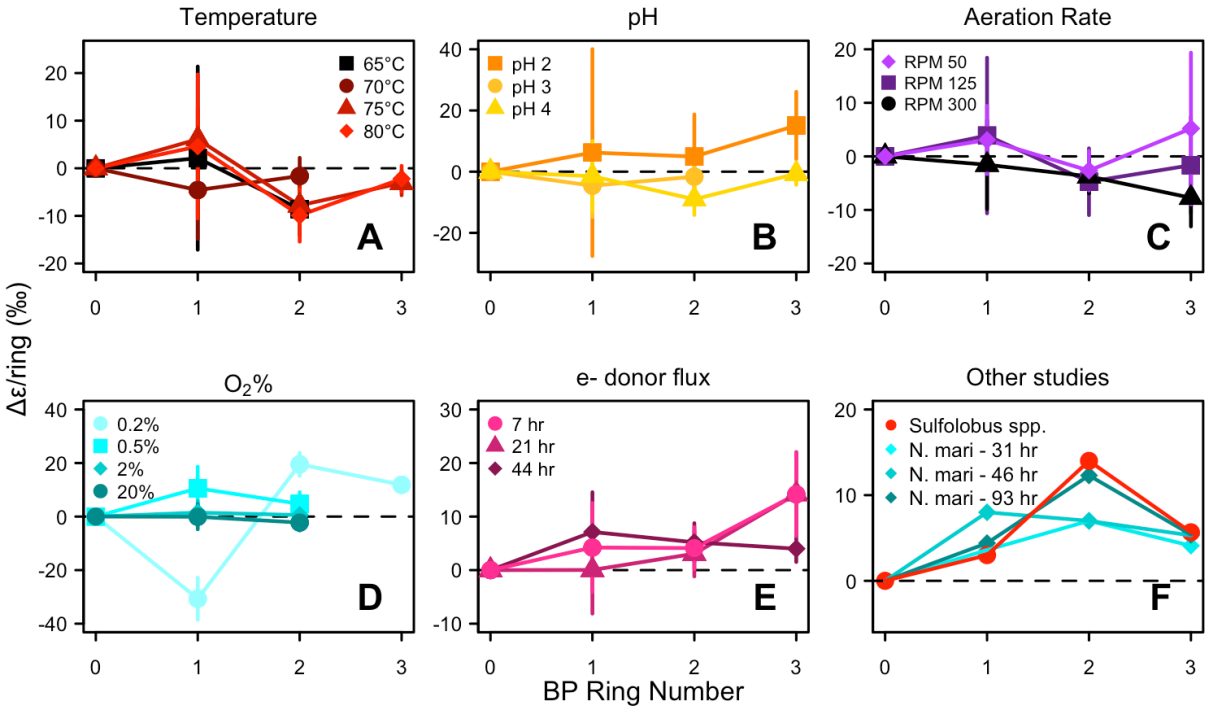

Fig. 3. (**A-E**) Ring difference (Δε/ring, ‰) for individual biphytanes in each environmental condition experiment. BP-0 has a Δε/ring of 0 by definition and is shown for reference. BP-3 was not recovered from every treatment. Note the axes are scaled differently for each plot. Points represent mean of biological and technical replicates for each treatment level. (**F**) Ring difference for biphytanes examined in other studies. Blue diamonds are *N. maritimus* from Leavitt et al., 2023; red squares are *Sulfolobus* sp. from Kaneko et al., 2011. Kaneko et al., also recovered BP-4 from *Sulfolobus* spp. (data not shown); the Δε/ring for BP-4 is 11.7 ‰.

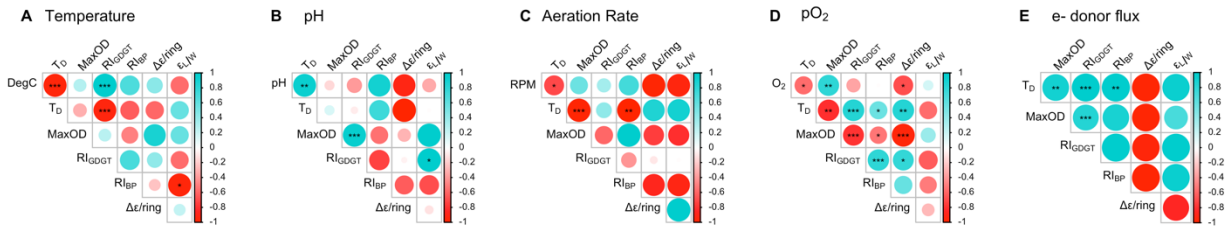

Fig. 4. Correlation matrices showing linear relationships among environmentally manipulated parameters, growth statistics (doubling time (T_D) and maximum OD_{600}), mean cyclization of lipids (RI-GDGT and RI-BP), ring difference, and abundance weighted mean $^2\varepsilon_{L/W}$ for (**A**) temperature, (**B**) pH, (**C**) aeration rate, (**D**) O_2 mixing ratio, and (**E**) electron donor flux. Notably, mean $^2\varepsilon_{L/W}$ values do not show a strong linear correlation to any other measured parameter, indicating that environmental conditions, growth statistics, and mean cyclization do not significantly influence the degree of lipid/water fractionation in *S. acidocaldarius*. Circle color and size indicate the strength and direction (blue = correlated, red = anticorrelated) of the relationship. Significance levels: * $p < 0.05$, ** $p < 0.001$, *** $p < 0.0001$. Circles without a star indicate the relationship is not statistically significant.

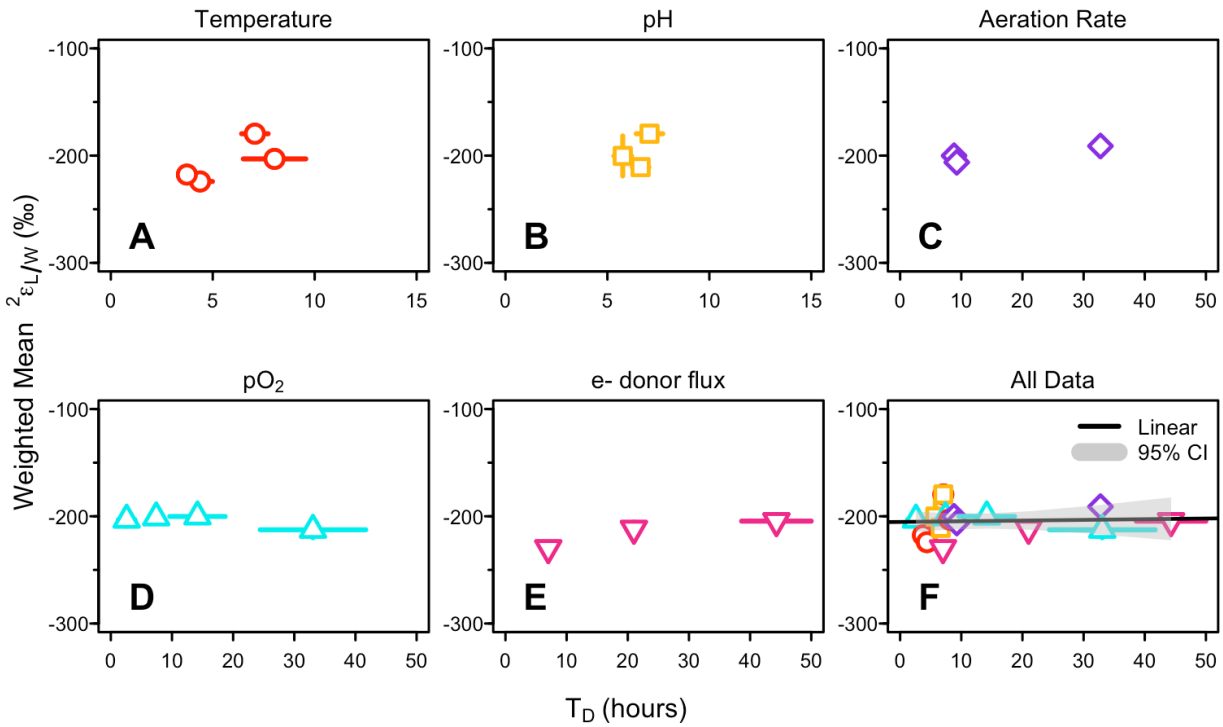

Fig. 5. The abundance weighted H-isotope fractionation ($^{2}\varepsilon_{L/W}$) between growth water and biphytanes (BPs) in response to doubling time (hours) in each individual environmental condition experiment (**A-E**) and pooled across all experiments (**F**). When data from all environmental control experiments is pooled, there is no relationship between doubling time (hours) and abundance weighted mean $^{2}\varepsilon_{L/W}$. Points represent mean of biological and technical replicates for each treatment level. Error bars represent propagated error associated with BP abundance measurements, BP-δ^{2}H measurements, and weighted mean $^{2}\varepsilon_{L/W}$ calculations; bars are smaller than the symbols in many cases.

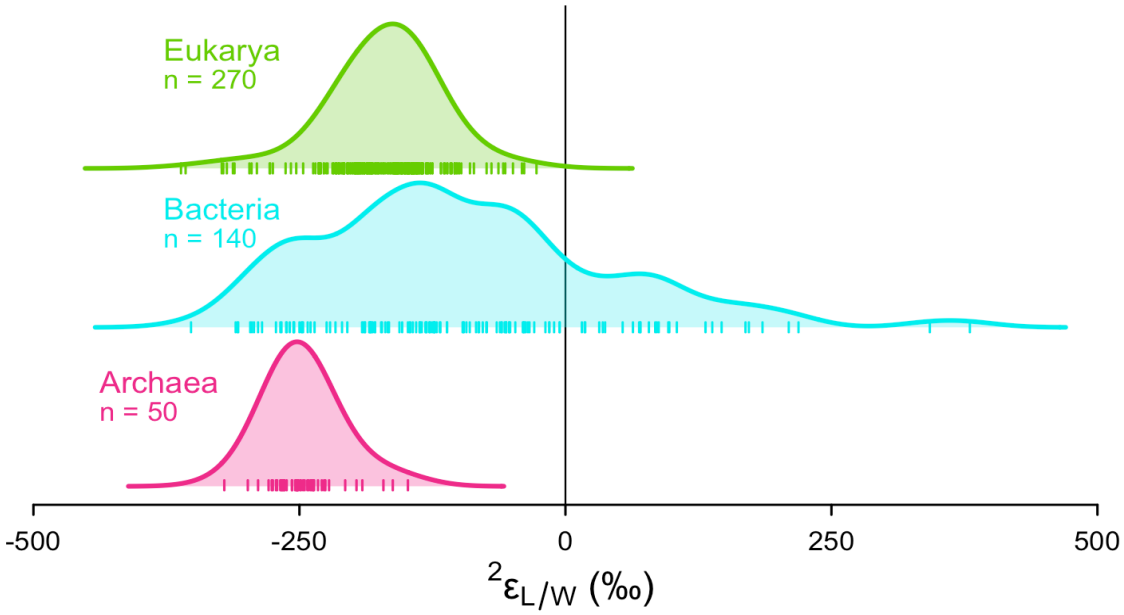

Fig. 6. Distributions of $^{2}\varepsilon_{L/W}$ values from culturing studies that measured $^{2}\varepsilon_{L/W}$ for eukaryotic phototrophs (green; n = 270), bacteria (blue; n = 140 measurements), and archaeal cultures (pink; n = 50 measurements). Tick marks show individual values. The archaeal studies include measurements of phytanes and biphytanes from *Sulfolobus* sp. (Kaneko et al., 2011), *M. barkeri* (Wu et al., 2020), *N. maritimus* (Leavitt et al., 2022), and *Acidianus* sp. DS80, *A. fulgidus*, and *Metallosphaera sedula* (Rhim et al., 2023). Data for eukaryotes and bacteria redrawn from Rhim et al., (2023), Figure 6. Eukarya data includes measurements for acetogenic and isoprenoid lipids. Bacterial data includes fatty acids synthesized by multiple metabolisms (e.g., aerobic and anaerobic heterotrophy, aerobic and anaerobic chemoautotrophy, and photoautotrophy).

Supplemental Information for

Lipid hydrogen isotope compositions primarily reflect growth water in the model archaeon *Sulfolobus acidocaldarius*

Carolynn M. Harris#, Sebastian Kopf, Jeemin H. Rhim, Alec Cobban, Felix J. Elling, Xiahong Feng, Jamie McFarlin, Yuki Weber , Yujiao Zhang, Alice Zhou, Harpreet Batther, Ann Pearson, William D. Leavitt

Address correspondence to Carolynn M. Harris**,** carolynn.m.harris.gr@dartmouth.edu

Supplementary Information Text

S1. Methods for ^2H_2O-Labeled Water Experiment

To test the incorporation of H derived from water into lipids, we cultured *S. acidocaldarius* on media prepared with either natural abundance water (-49 ‰), with ^{2}H-depleted water (-361 ‰; filtered Antarctic ice-core melt water, courtesy of Erich Osterburg) or with ^{2}H-enriched water (+415 ‰; achieved via addition of 99.9% D_2O) (**Table S1**). Culture media was prepared following the Brock recipe in Wagner et al. (2012), where the complex carbon sources in the media were replaced by 16.7 mmol L^{-1} (0.3% w/v) glucose and 4.0 mmol L^{-1} (0.1% w/v) NZ-amine as the sole organic substrates. Growth was monitored photometrically at regular intervals throughout each experiment by measuring the optical density (i.e., absorbance at 1 cm pathlength) of a culture aliquot at 600 nm (OD_{600}) on a spectrophotometer.

Batch experiments were performed in temperature-controlled, shaking incubators (Innova-42, Eppendorf) in 250 mL Erlenmeyer flasks containing 125 mL media covered with loose plastic caps to reduce evaporation. Evaporation was further reduced by maintaining a 2L tray of water in the incubator to humidify the atmosphere. Environmental conditions were 70°C, pH 3, and 100 RPM shaking speed. All experiments were performed in triplicate. Biomass samples were collected in mid-exponential phase by centrifuging (3214 x *g*; Eppendorf 5810 R, S-4-104 rotor) 50 mL of culture for 15 minutes at 4 °C, the resulting cell pellets were stored at -80 °C until lipid extraction. Isoprenoid BP chains were extracted and analyzed as described in the main text. The methods used to determine H-isotope composition of lipids, media waters, and substrates are as described in the main text. ^{2}H-labeled waters were diluted with standards of known isotopic composition prior to analysis. The δ^2H composition of glucose was -44.5 ± 2.9 ‰.

S2. *S. acidocaldarius* H-isotope mixing model

Batch experiments tested the incorporation of water-derived H into biphytane lipids of *S. acidocaldarius*. Doubling times for all treatments ranged from 7 to 11 hours and were unaffected by the δ^2H compositions of growth water (**Table S1, FIG S6A,B**). These rates are consistent with doubling times reported for *S. acidocaldarius* in Cobban et al. (2020) and Zhou et al. (2020). In all samples, BP-1 and BP-2 are the most abundant, and BP-3 is consistently < 10% of the total BP pool; BP distributions were not impacted by δ^2H_{Water} (**Table S2, FIG S6C**). The δ^2H composition of BPs was strongly correlated to the δ^2H compositions of growth water with a consistent large and negative offset ($R^2 > 0.999$, $p < 0.001$) (**FIG S7A**).

Biphytane δ^2H values reflect the sum of distinct isotope fractionations between the lipid product and the two potential sources of hydrogen for heterotrophs – water and the organic substrate used for growth. This relationship can be written as an isotopic mass balance equation, originally developed

by Zhang et al. (2009), that describes heterotrophic H metabolism as a two-source mixing model (**Eq. S1**). The net fractionations between lipids and each external H source are considered separately in the following model:

Eq. (S1) $$R_L = f_W \cdot {}^2\alpha_{L/W} \cdot R_W + f_S \cdot {}^2\alpha_{L/S} \cdot R_S$$

where R_L is the abundance weighted mean $^2H/^1H$ ratios of BP-0, -1, -2, and -3, R_W is the $^2H/^1H$ ratio of media water, and R_S is the $^2H/^1H$ ratios of the organic substrate (e.g., glucose). f_W and f_S are the fractions of lipid-bound H derived from water and substrate, respectively. ${}^2\alpha_{L/W}$ represents the net isotope fractionation factor between lipid and water and ${}^2\alpha_{L/S}$ between lipid and substrate. This model illustrates the overall isotopic relationship between lipids and external hydrogen sources without implying that these sources are directly involved in lipid biosynthesis. For example, glucose may contribute H to lipids through metabolic intermediates, even though it does not directly participate in the biosynthetic reactions.

Our experimental cultures varied R_W while holding R_S constant. The other terms of this model can be constrained by regressing R_L values on R_W. The slope of this regression is equivalent to [$f_W \cdot {}^2\alpha_{L/W}$], and the y-intercept is equivalent to [$(1- f_W) \cdot {}^2\alpha_{L/W} \cdot R_S$]. Because f_W is unknown in heterotrophic growth conditions, we explore the possible range of fractionation factors – ${}^2\alpha_{L/W}$ and ${}^2\alpha_{L/S}$ – by varying f_W to range from 0 to 1 (Zhang et al. 2009) (**FIG S7B**). As the fraction of H sourced from water (f_W) increases, the expected lipid/water fractionation value (${}^2\alpha_{L/W}$) becomes larger and more negative. We can further constrain the likely values of f_W by assuming that lipid/water fractionation is negative (${}^2\alpha_{L/W} < 0$; a normal kinetic isotope fractionation). This is a conservative assumption given all previous research on archaea, including the *Sulfolobus* genus, have reported large, negative values for lipid/water fractionation (Kaneko et al. 2011; Rhim et al. 2024). Also, reports for direct water incorporation in bacteria estimate that ${}^2\alpha_{L/W} = 0.9$ (Zhang et al. 2009; Wijker et al. 2019). With this additional assumption, we can conclude that when *S. acidocaldarius* is grown heterotrophically on a simple sugar, the majority of lipid-H (≥ 56 ± 1 %) is derived from water H, rather than from substrate H.

S3. Discussion of H-isotope mixing model

This study aimed to determine the extent to which archaeal biphytane-δ^2H values record the δ^2H value of environmental water. In heterotrophic archaea, lipid-bound H can originate from water or the organic substrate used for growth, with intracellular hydride carriers, such as NADPH, mediating the incorporation of H from both sources into lipids (Zhang et al. 2009; Dirghangi and Pagani 2013; Wijker et al. 2019). In heterotrophs, the NADPH incorporated into lipid products inherits some H from the available organic substrate(s). Our experiments show that when *S. acidocaldarius* is grown heterotrophically on a simple sugar (glucose), the weighted mean δ^2H composition of biphytane lipids is strongly correlated with δ^2H_{Water}, indicating a strong first-order control. Isotope mass balance

modeling suggests water contributes at least 56 ± 1% of the total H flux to lipids (**FIG. S7B**). One limitation to this approach is that our experiments were conducted in a semi-defined rich-media, experiments in a defined media using a single carbon source (e.g., glucose only) with ^{2}H-labels at particular sites on the molecule will better constrain the relative contribution of substrates and water to lipid products (Harris et al. 2022).

This magnitude of water contribution to lipids in *S. acidocaldarius* aligns with a recent study on the metabolically-flexible anaerobe, *Archaeoglobus fulgidus*, which demonstrates that at least 50% of biphytane-bound H reflects $\delta^{2}H_{Water}$ when grown heterotrophically, compared to over 80% when grown autotrophically (Rhim et al. 2023). Similarly the aerobic and heterotrophic *H. marismortui* synthesizes diether lipids (archaeol) with δ^{2}H compositions tightly correlated with $\delta^{2}H_{Water}$, indicating a first order control, but R_{Lipid} vs. R_{Water} regression parameters and fractionation constraint curves differ when grown on different carbon sources (Dirghangi and Pagani 2013). Applying the assumption that $^{2}\alpha_{L/W} < 1$ (a normal isotope effect) suggests that *H. marismortui* derives >78%, >80%, and >12% of archaeol-H from water when grown on pyruvate, succinate, and glucose, respectively. This pattern cannot be explained by a simple inheritance of substrate δ^{2}H value (pyruvate = -97‰; succinate = -382‰; and glucose = -61‰) and is likely attributable to large fractionations associated with substrate metabolism and other processes that impact the δ^{2}H composition of NADPH (Dirghangi and Pagani 2013).

The large portion of lipid-H that appears to be sourced from water in heterotrophic archaea and in a subset of bacteria (notably heterotrophs in energetically stressful conditions, such as anaerobiosis (Zhang et al. 2009; Dawson et al. 2015; Osburn et al. 2016) could reflect similarities in the physiology and/or ecology of these microbes. Archaea and these bacteria may use common biosynthetic pathways with enzymes that have large isotope effects (Rhim et al. 2024). Overall, this finding is consistent with the narrow range of $^{2}\varepsilon_{L/W}$ values observed for the Archaea relative to other domains.

Supplementary Tables

Table S1. Summary of culture conditions and descriptive growth statistics for *S. acidocaldarius* grown in media prepared with ^{2}H-labeled waters.

Table S2. Descriptive statistics for biphytanyl (BP) lipids derived from iGDGTs for *S. acidocaldarius* grown in media prepared with ^{2}H-labeled waters. Mean and sd include biological replication and technical replication (multiple injections). *N* = number of biological replicates in each treatment, *n* is the number of replicates analyzed for lipid composition.

Supplementary Figures

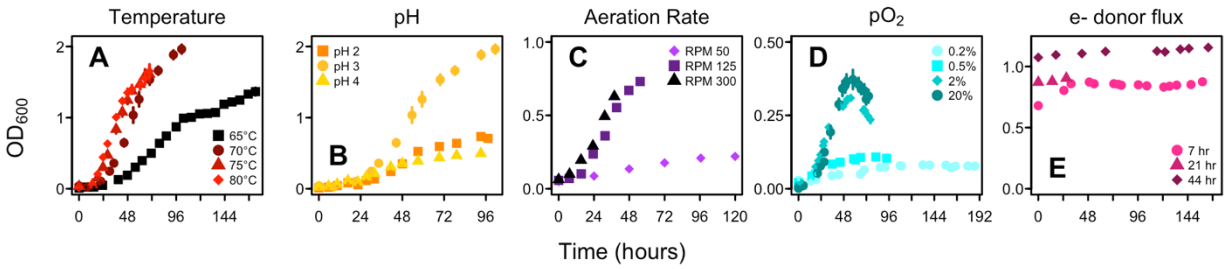

Fig S1. Growth curves for *S. acidocaldarius* grown under varying environmental conditions. Originally published in Cobban et al., 2020 (A-D) and Zhou et al., 2020 (E). Points and error bars represent mean and standard deviation of biological replicates for each treatment level. Error bars are smaller than the symbols in many cases.

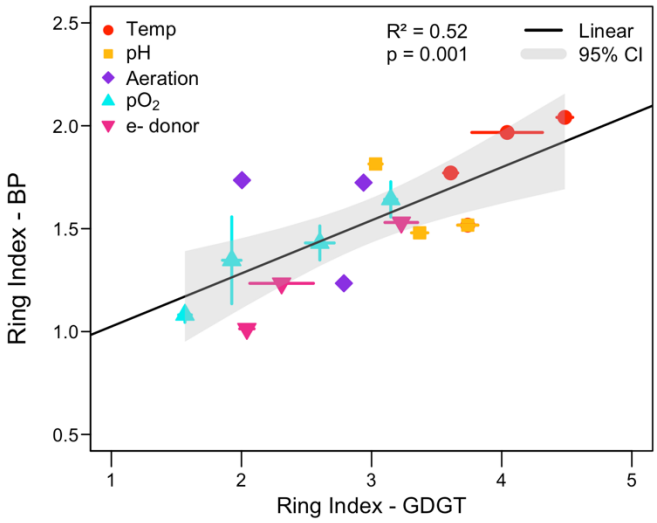

Fig S2. Correlation between Ring Indices for parent iGDGTs and derivatized biphytanes across all environmental condition experiments. Points and error bars represent mean and standard deviation of biological and technical replicates for each treatment level.

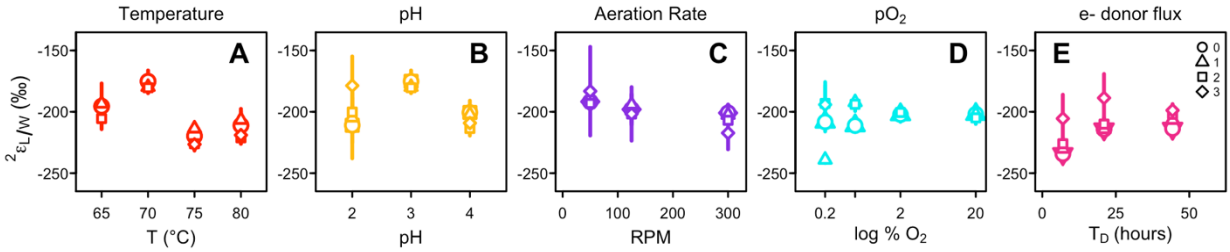

Fig S3. $^{2}\varepsilon_{L/W}$ values (‰) for individual biphytanes (BP-0 = circle; BP-1 = triangle; BP-2 = square; BP-3 = diamond) in response to each environmental condition (A-E). BP-3 was not recovered from every treatment. Points represent means and propagated error across biological and technical replicates.

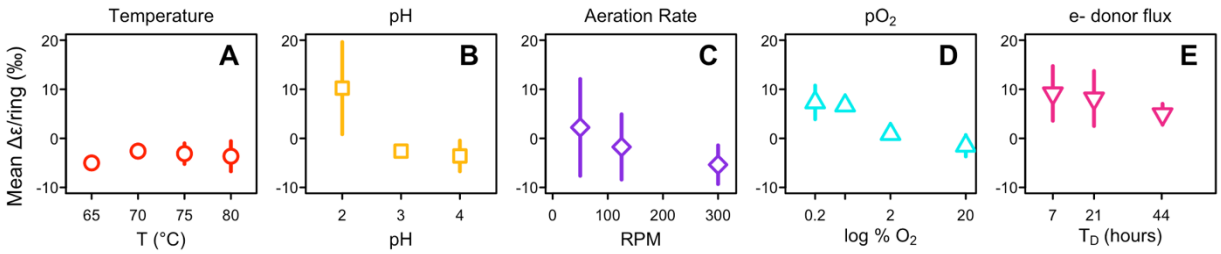

Fig S4. Mean ring difference (Δε/ring, ‰) in response to each environmental condition (A-E). Points show the mean and propagated error across biological and technical replicates.

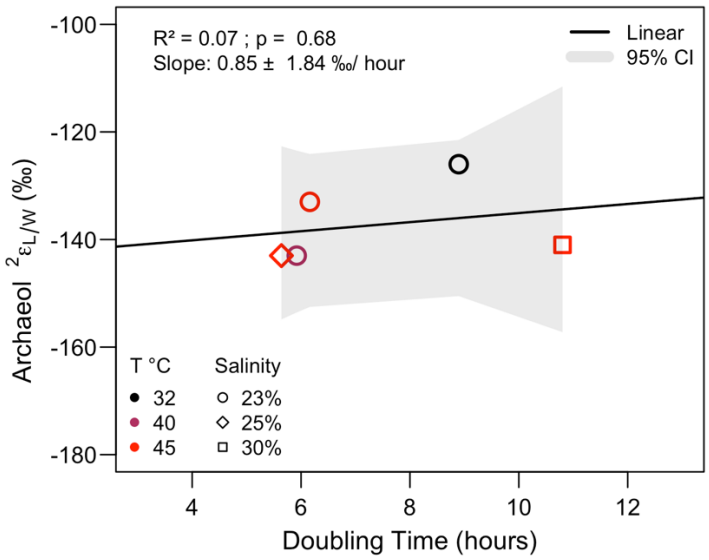

Fig S5. The relationship between doubling time and $^{2}\varepsilon_{L/W}$ for archaeol lipids isolated from experimental cultures of the halophile, *Haloarcula marismortui*, grown under different salinity (symbol shapes) and temperature (symbol color) regimes with yeast extract as the growth substrate (Dirghangi and Pagani, 2013).

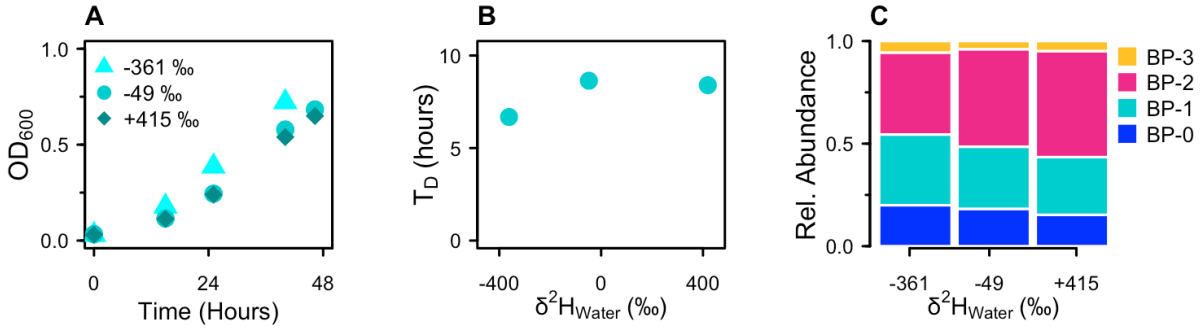

Fig S6. A) Growth curves, B) doubling times, and C) relative abundances of biphytane lipids derived from iGDGTs for *S. acidocaldarius* grown in Brock media with varying δ^2H_{Water}. Points and error bars represent the mean and standard error of biological triplicates. Error bars are smaller than the symbols.

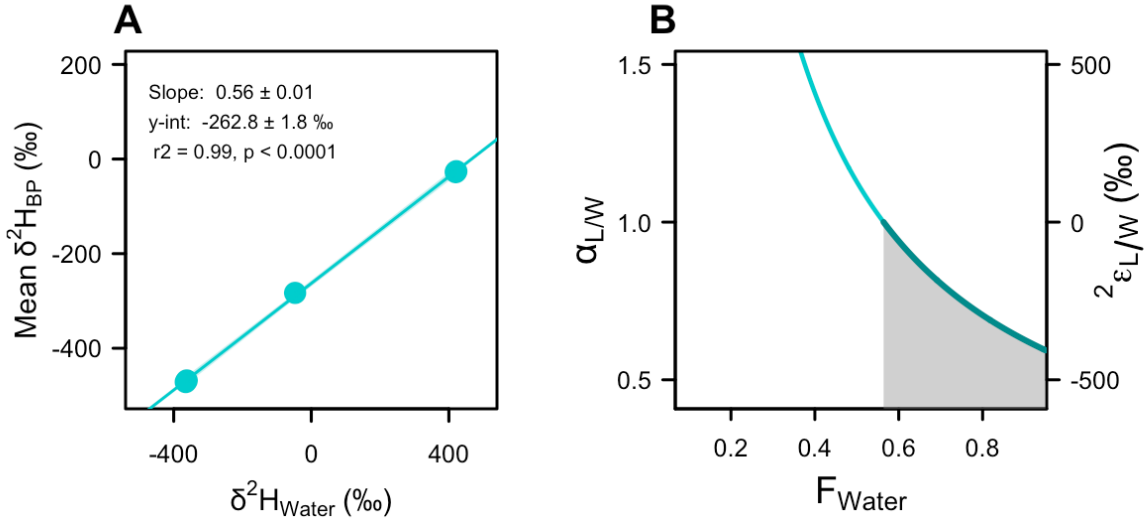

Fig S7. A) Regressions of R_{Lipid} on R_{Water} for the ^{2}H-labeled water experiment. Points show mean and standard error of biological triplicates. Error bars are smaller than symbols. 95% CI is thinner than the width of the regression line. R_{Lipid} represents abundance weighted mean R_{BP} values. [Note: axes are shown in per mil units for ease of interpretation. Regression parameters were calculated from *R* values]. B) Because the mass-balance model (Eq. S1) is under constrained, we cannot solve for an exact value of $^2\alpha_{L/W}$; this curve represents the fractionation factor that results from every possible value of f_{Water}. 95% CI is thinner than the width of the curve. We can constrain the most likely range of f_{Water} values by assuming a normal kinetic isotope effect where lipids are ^{2}H-depleted relative to source water (e.g., $^2\alpha_{L/W} < 1$; shaded region of the curve). To satisfy the assumption that $^2\alpha_{L/W} < 1$, environmental water must supply at least 56 ± 1 % of H flux to lipid products.

SI References

Cobban A, Zhang Y, Zhou A, et al (2020) Multiple environmental parameters impact core lipid cyclization in Sulfolobus acidocaldarius. Environmental Microbiology 1–28

Dawson KS, Osburn MR, Sessions AL, Orphan VJ (2015) Metabolic associations with archaea drive shifts in hydrogen isotope fractionation in sulfate-reducing bacterial lipids in cocultures and methane seeps. Geobiology 13:462–477. https://doi.org/10.1111/gbi.12140

Dirghangi SS, Pagani M (2013) Hydrogen isotope fractionation during lipid biosynthesis by Tetrahymena thermophila. Organic Geochemistry 64:105–111. https://doi.org/10.1016/j.orggeochem.2013.09.007

Harris C, Rhim J, Zhang Y, et al (2022) Determining controls on hydrogen isotope fractionation in archaeal tetraether lipids in a thermoacidophilic archaeal heterotroph. In: Goldschmidt2022 abstracts. European Association of Geochemistry, Honolulu, HI, USA

Kaneko M, Kitajima F, Naraoka H (2011) Stable hydrogen isotope measurement of archaeal ether-bound hydrocarbons. Organic Geochemistry 42:166–172. https://doi.org/10.1016/j.orggeochem.2010.11.002

Osburn MR, Dawson KS, Fogel ML, Sessions AL (2016) Fractionation of hydrogen isotopes by sulfate- and nitrate-reducing bacteria. Frontiers in Microbiology 7:1–16. https://doi.org/10.3389/fmicb.2016.01166

Rhim JH, Zhou A, Amenabar MJ, et al (2024) Mode of carbon and energy metabolism shifts lipid composition in the thermoacidophile *Acidianus*. Appl Environ Microbiol e01369-23. https://doi.org/10.1128/aem.01369-23

Wagner M, Van Wolferen M, Wagner A, et al (2012) Versatile Genetic Tool Box for the Crenarchaeote Sulfolobus acidocaldarius. Front Microbio 3:. https://doi.org/10.3389/fmicb.2012.00214

Wijker RS, Sessions AL, Fuhrer T, Phan M (2019) 2H/1H variation in microbial lipids is controlled by NADPH metabolism. Proceedings of the National Academy of Sciences of the United States of America 116:12173–12182. https://doi.org/10.1073/pnas.1818372116

Zhang X, Gillespie AL, Sessions AL (2009) Large D/H variations in bacterial lipids reflect central metabolic pathways. Proceedings of the National Academy of Sciences of the United States of America 106:12580–12586. https://doi.org/10.1073/pnas.0903030106

Zhou A, Weber Y, Chiu BK, et al (2020) Energy flux controls tetraether lipid cyclization in Sulfolobus acidocaldarius. Environmental Microbiology 22:343–353. https://doi.org/10.1111/1462-2920.14851

Experiment	N	Growth Conditions					Growth Rate (hour^{-1})		Doubling Time (Hours)		Max OD	
		Treatment	T°C	pH	RPM*	O_2 %	Mean	sd	Mean	sd	Mean	sd
Temp (°C)	5	65	65	3	200	air	0.09	0.02	8.03	1.53	1.37	0.12
	5	70	70	3	200	air	0.10	0.01	7.07	0.65	1.96	0.14
	5	75	75	3	200	air	0.16	0.02	4.38	0.60	1.61	0.23
	5	80	80	3	200	air	0.19	0.01	3.73	0.19	1.65	0.21
pH	5	2	70	2	200	air	0.12	0.01	5.75	0.43	0.71	0.04
	5	3	70	3	200	air	0.10	0.01	7.07	0.65	1.96	0.14
	5	4	70	4	200	air	0.10	0.01	6.63	0.41	0.49	0.03
Shaking (RPM)	5	50	70	3	50	air	0.02	0.00	32.75	1.50	0.22	0.01
	5	125	70	3	125	air	0.08	0.00	8.82	0.51	0.73	0.01
	5	300	70	3	300	air	0.07	0.00	9.26	0.25	0.63	0.02
O_2 mixing ratio (%)	3	0.2%	70	3	200	0.2	0.02	0.00	33.05	8.64	0.08	0.00
	3	0.5%	70	3	200	0.5	0.05	0.02	14.17	4.54	0.10	0.00
	3	2%	70	3	200	2	0.09	0.01	7.42	0.63	0.24	0.02
	3	20%	70	3	200	20	0.34	0.21	2.58	1.36	0.32	0.04
e- donor flux (T_D, hours)	6	7	70	2.25	200	20	0.14	0.00	7.00	0.09	0.84	0.10
	9	21	70	2.25	200	20	0.05	0.00	21.00	0.45	0.88	0.03
	6	44	70	2.25	200	20	0.02	0.00	44.30	5.68	1.12	0.04

				BP-0						BP-1								BP-2								BP-3								Abundance weighted mean						Ring Index	
Experiment	Treatment	N	n	Rel Abund	sd	δ2HBP (‰)	sd	^{2}εL/W (‰)	sd	Rel Abund	sd	δ2HBP (‰)	sd	^{2}εL/W (‰)	sd	Δε/ring	sd	Rel Abund	sd	δ2HBP (‰)	sd	^{2}εL/W (‰)	sd	Δε/ring	sd	Rel Abund	sd	δ2HBP (‰)	sd	^{2}εL/W (‰)	sd	Δε/ring	sd	δ2HBP (‰)	sd	^{2}εL/W (‰)	sd	Δε/ring	sd	mean	sd
Temp (ºC)	65	5	1	0.1	0.0	-233.8	17.8	-195.5	18.7	0.1	0.0	-231.8	4.5	-193.4	4.8	2.1	19.3	0.8	0.0	-243.3	3.0	-205.5	3.2	-8.6	5.5	0.0	0.0							-241.0	5.3	-203.1	5.3	-5.0	0.0	1.8	0.0
	70	5	1	0.1	0.0	-220.6	8.4	-175.2	8.9	0.3	0.0	-224.9	4.9	-179.7	5.1	-4.6	10.3	0.6	0.1	-225.5	3.0	-180.4	3.1	-1.6	3.8	0.0	0.0							-224.8	4.4	-179.6	4.4	-2.6	0.0	1.5	0.2
	75	5	1	0.1	0.0	-262.0	4.3	-219.7	4.6	0.1	0.0	-256.2	4.5	-213.6	4.7	6.1	6.6	0.6	0.0	-268.0	5.3	-226.0	5.6	-7.8	4.1	0.2	0.0	-268.4	3.8	-226.5	4.0	-3.1	2.6	-266.2	4.8	-224.1	4.8	-3.1	2.1	2.0	0.1
	80	5	1	0.1	0.0	-252.7	12.8	-211.1	13.5	0.1	0.0	-248.3	6.5	-206.5	6.9	4.6	15.1	0.5	0.0	-262.2	4.6	-221.2	4.9	-9.9	5.5	0.3	0.0	-260.1	2.7	-219.0	2.9	-2.2	2.7	-258.9	5.5	-217.7	5.5	-3.6	3.1	2.0	0.0
pH	2	5	1	0.2	0.0	-258.1	25.4	-211.0	27.0	0.3	0.0	-252.2	19.1	-204.7	20.3	6.2	33.8	0.4	0.0	-248.0	10.8	-200.2	11.4	4.9	13.8	0.2	0.0	-227.8	22.4	-178.7	23.8	15.1	11.0	-248.1	##	-200.3	18.6	10.2	9.4	1.5	0.0
	3	5	1	0.1	0.0	-220.6	8.4	-175.2	8.9	0.3	0.0	-224.9	4.9	-179.7	5.1	-4.6	10.3	0.6	0.1	-225.5	3.0	-180.4	3.1	-1.6	3.8	0.0	0.0							-224.8	4.4	-179.6	4.4	-2.6	0.0	1.5	0.2
	4	5	1	0.1	0.0	-249.2	9.0	-200.6	9.6	0.1	0.0	-250.6	5.9	-202.0	6.3	-1.5	11.5	0.7	0.0	-261.5	5.5	-213.6	5.8	-9.0	5.1	0.1	0.0	-257.3	6.5	-209.2	6.9	-0.7	3.6	-258.9	5.9	-210.8	5.9	-3.6	3.1	1.8	0.0
Shaking (RPM)	50	5	1	0.2	0.0	-230.2	3.3	-191.7	3.4	0.4	0.0	-227.2	5.1	-188.6	5.4	3.1	6.4	0.4	0.0	-231.6	4.1	-193.2	4.3	-2.7	3.7	0.0	0.0	-222.0	34.4	-183.2	36.1	5.2	14.2	-229.5	6.5	-191.1	6.5	2.2	9.9	1.2	0.0
	125	5	1	0.1	0.0	-235.2	11.9	-198.0	12.5	0.2	0.0	-231.5	7.1	-194.1	7.5	3.9	14.5	0.7	0.0	-238.7	6.6	-201.8	7.0	-4.7	6.2	0.1	0.0	-238.7	20.8	-201.7	21.8	-1.6	9.0	-237.2	8.5	-200.1	8.6	-1.8	6.7	1.7	0.0
	300	5	1	0.1	0.0	-238.4	6.5	-200.9	6.8	0.2	0.0	-239.9	4.6	-202.4	4.8	-1.6	8.3	0.7	0.0	-244.1	2.1	-206.9	2.2	-3.7	3.2	0.1	0.0	-254.0	12.7	-217.3	13.3	-7.7	5.4	-243.5	4.4	-206.2	4.4	-5.4	3.9	1.7	0.0
O_2 mixing ratio (%)	0.2%	3	2	0.1	0.0	-244.1	1.8	-208.2	7.8	0.3	0.0	-274.7	6.9	-239.1	2.7	-30.7	5.2	0.6	0.1	-231.0	13.4	-193.2	17.5	19.5	2.8	0.1	0.0	-230.6	9.0	-194.1	15.4	11.9	1.2	-248.2	7.5	-212.6	7.5	7.3	3.4	1.6	0.3
	0.5%	3	1	0.1	0.0	-254.9	5.0	-211.2	5.3	0.4	0.1	-237.1	4.4	-192.2	4.7	10.6	8.1	0.5	0.1	-238.6	5.3	-193.8	5.6	4.7	4.4	0.0	0.0							-244.4	5.1	-200.2	5.1	6.7	0.0	1.4	0.4
	2%	3	3	0.2	0.0	-243.2	5.5	-202.2	6.0	0.4	0.0	-241.8	2.2	-200.8	3.6	1.5	0.0	0.3	0.0	-241.5	4.1	-200.5	5.0	0.6	0.2	0.0	0.0							-242.0	5.2	-201.0	5.2	0.9	0.9	1.1	0.4
	20%	3	3	0.2	0.0	-242.6	0.5	-202.0	0.7	0.4	0.0	-242.7	4.2	-202.0	5.0	-0.1	1.5	0.4	0.0	-245.5	4.5	-205.0	5.0	-2.2	0.9	0.1	0.1							-243.8	6.0	-203.2	6.0	-1.5	2.2	1.3	0.8
e- donor flux (T_D, hours)	7	6	1	0.3	0.0	-280.0	6.7	-234.3	7.1	0.4	0.0	-276.0	4.0	-230.1	4.3	4.2	8.3	0.3	0.0	-272.2	5.9	-226.0	5.0	4.1	3.9	0.0	0.0	-252.8	16.8	-205.5	19.4	14.2	7.8	-275.7	5.7	-229.8	5.7	9.2	5.6	1.0	0.0
	21	9	1	0.2	0.0	-261.0	5.6	-214.2	5.9	0.4	0.0	-260.9	5.2	-214.1	5.6	0.0	8.2	0.4	0.0	-257.1	4.7	-210.1	5.0	3.1	4.2	0.0	0.0	-237.0	18.4	-188.7	19.5	14.2	7.9	-258.6	6.1	-211.7	6.1	8.1	5.6	1.2	0.0
	44	6	1	0.1	0.0	-252.7	4.4	-213.6	4.6	0.3	0.0	-245.9	5.5	-206.5	5.8	7.1	7.4	0.5	0.0	-241.6	2.9	-202.0	3.1	5.2	3.6	0.1	0.0	-238.6	4.8	-198.8	5.1	4.0	2.5	-244.0	4.1	-204.5	4.1	4.9	2.1	1.5	0.0